Article

Not peer-reviewed version

Drainage Duration Variability and PALSAR-2 Sensitivity to Rice Field Water Status: Insights from Large-Scale In Situ Water-Level Observations

Xiao Jin *, Muditha Madusanka Dantanarayana , Alexis Declaro , Shinjiro Kanae , Alvin C.G. Varquez

Posted Date: 5 May 2026

doi: 10.20944/preprints202604.2223.v1

Keywords: alternate wetting and drying (AWD); in situ water-level monitoring; drainage duration; satellite remote sensing; Synthetic Aperture Radar (SAR); ALOS-2 PALSAR-2; inundation; monitoring; reporting and verification (MRV)

 doi:10.20944/preprints202604.2223.v1

Article

Drainage Duration Variability and PALSAR-2 Sensitivity to Rice Field Water Status: Insights from Large-Scale In Situ Water-Level Observations

Xiao Jin [1,*], Muditha Madusanka Dantanarayana [2], Alexis Declaro [3], Shinjiro Kanae [2] and Alvin C.G.Varquez [1]

[1] Department of Transdisciplinary Science and Engineering, School of Environment and Society, Institute of Science Tokyo, Ookayama, Meguro, 152-8550, Tokyo, Japan
[2] Department of Civil and Environmental Engineering, School of Environment and Society, Institute of Science Tokyo, Meguro 152-8550, Tokyo, Japan
[3] Creattura Co. Ltd., Chuo-ku, Tokyo 103-0006, Japan
* Correspondence: jin.x.ac@m.titech.ac.jp; Tel.: +81-80-6580-1110

Abstract

Achieving scalable monitoring of Alternate Wetting and Drying (AWD) for methane mitigation in rice cultivation depends on establishing field benchmarks for drainage behavior and demonstrating that satellite observations can reliably detect corresponding changes in water status. We analyzed about two million high-frequency in situ water-level observations from hundreds of sensors deployed in rice fields across Philippines and Japan to quantify drainage duration from near-surface conditions to 15 cm below the soil surface and to test the sensitivity of open-access PALSAR-2 dual-polarization L-band SAR to vertical water level variations. Across 564 drainage events, the median drainage duration was 19.0 h, and only 0.9% of events exceeded 240 h, indicating that drainage happens generally within a day. Drainage duration varied markedly by region and season, with median values ranging from 10.6 h in Pangasinan wet-season events to 72.6 h in Cagayan dry-season events; multiple drainage events occurred in 48.0% of Philippine dry-season fields but only 21.6% of wet-season fields. PALSAR-2 data shows a statistical significance in detecting inundation at Mid crop growth stage with cross-polarization band, but the significant overlap induce challenges in operational applications. These results provide empirical benchmarks for AWD-related drainage dynamics while showing that dual-polarization PALSAR-2 alone is unlikely to support robust field-scale monitoring of rice-field water status.

Keywords: alternate wetting and drying (AWD); in situ water-level monitoring; drainage duration; satellite remote sensing; Synthetic Aperture Radar (SAR); ALOS-2 PALSAR-2; inundation; monitoring; reporting and verification (MRV)

1. Introduction

Irrigated rice systems are an important source of anthropogenic methane because prolonged flooding creates anaerobic soil conditions that are conducive to methanogenesis [1]. Recent global methane budgets estimate that rice paddies emitted approximately 32 [25–37] Tg CH_4 yr^{-1} during 2010–2019, accounting for approximately 9% of global anthropogenic CH_4 emissions, with the largest contributions concentrated in Asia [2]. Consequently, water management during the cultivation period has become a central component of rice methane accounting and mitigation. The Intergovernmental Panel on Climate Change (IPCC) inventory framework distinguishes continuously flooded, single-drainage, and multiple-drainage irrigated rice systems, assigning lower CH_4 scaling factors to single and multiple drainage than to continuous flooding [3]. Reliable monitoring, reporting, and verification (MRV) of drainage practices is therefore essential for translating water-management interventions into credible climate mitigation outcomes.

 doi:10.20944/preprints202604.2223.v1

Alternate Wetting and Drying (AWD) reduces CH_4 emissions by periodically interrupting flooded, anaerobic soil conditions. In agronomic practice, safe AWD is commonly implemented by allowing ponded water to disappear and re-irrigating when the perched water table falls to approximately 15 cm below the soil surface [4,5,5–7]. This −15 cm reference has also been used in experimental AWD studies in Southeast Asia, including treatments in which fields are re-irrigated when water level naturally declines to this set depth threshold below the soil surface [8–10]. Meta-analytic evidence shows that the CH_4 mitigation effect of non-continuous flooding increases with the number of drying events, soil-drying severity, and the total number of unflooded days, while yield penalties are mainly associated with more severe drying rather than mild AWD conditions [11,12]. This makes the transition from the soil surface to −15 cm a hydrologically meaningful interval for both methane mitigation and agronomic risk management.

Previous AWD studies and extension guidelines have commonly represented irrigation management using either water-level thresholds or prescribed drying intervals. In threshold-based approaches, fields are re-irrigated when water levels fall to a specified depth below the soil surface [13,14], whereas interval-based approaches define drying cycles based on elapsed time after the disappearance of ponded water [15] or fixed irrigation schedules [16–18]. While such rule-based approaches are useful for controlled implementation, they do not provide empirical information on how long fields take to drain to critical depths (e.g., −15 cm) and may fail to capture the variability of water-level dynamics under real-world conditions, where drainage and re-irrigation are influenced by local hydrology, rainfall, and farmer decision-making. Because drainage duration emerges from interacting hydrological and management processes, it is unlikely to be uniform across operational rice systems and is expected to vary with field and environmental conditions. Field water recession reflects not only irrigation scheduling, but also rainfall, antecedent soil wetness, soil permeability, groundwater depth, field leveling, bund and outlet conditions, and local water availability [5,19]. Recent landscape-scale work in Eastern India further showed that monsoon-season rice fields can exhibit multiple distinct hydrologic patterns within the same landscape, and that these patterns are not stable across years [20]. These findings highlight the need for a field-level analysis of how drainage duration and drainage recurrence vary across fields, soils, regions, and seasons. Translating this need into scalable monitoring frameworks, however, requires observation systems that extend beyond in situ measurements.

Although in situ water level measurements provide direct and high-frequency observations of field hydrology, their spatial coverage is limited, particularly challenged in scaling support MRV frameworks. Remote sensing observations, if they have been proven to be sensitive to relevant hydrological states, offer a pathway for scalable and independent confirmaation of AWD practices. Synthetic Aperture Radar (SAR) has been widely recognized as a suitable tool for monitoring paddy fields and is being studied to detect inundation status in paddy fields due to its sensitivity to surface properties and its all-weather imaging capability. This is significant for paddy related applications where the wet season in which the paddy is mainly grown is dominated by cloudy days [21–25]. In particular, L-band SAR systems such as Phased Array type L-band SAR 2 (PALSAR-2) onboard the Advanced Land Observing Satellite 2 (ALOS-2) offer distinct advantages over C-band systems like Sentinel-1, for applications over paddy fields. The longer wavelength of the L-band (23 cm) allows a deeper penetration through the rice canopy, enhancing the detectability of standing water beneath the vegetation even during later growth stages [21,26], with a higher sensitivity to water conditions [27]. While Quadruple (full; HH, HV, VV and VH) polarization SAR data enable detailed characterization of scattering mechanisms [21], open-access PALSAR-2 observations are primarily available in dual polarization. While dual-polarization SAR backscatter has been widely applied to mapping paddy extent and inundation [28,29], its sensitivity to hydrological dynamics relevant to AWD, particularly subsurface water-level transitions, remains less well understood. This is especially important for AWD applications, where critical thresholds for CH_4 mitigation depend not only on surface inundation but also on the depth of soil drying.

 doi:10.20944/preprints202604.2223.v1

Therefore, this study combines comprehensive drainage duration analysis and preliminary satellite remote sensing feasibility analysis to address both the process understanding and the scalability challenge of AWD monitoring. We leverage more than two million high-frequency in situ water-level records collected from hundreds of rice fields across the Philippines and Japan, enabling direct observation of fine-scale drainage processes and their variability across diverse climatic, soil, and management conditions. First, we analyze drainage duration variability under field conditions where water levels are not constrained by prescribed irrigation rules but instead reflect interacting hydrological processes. Using high-frequency in situ observations, we quantify the time required for water levels to decline from near-surface conditions to −15 cm, providing an empirical measure of drainage duration under these conditions. We further examine how these drainage dynamics vary across fields and seasons. Second, we use these in situ measurements as a reference to evaluate whether open-access PALSAR-2 dual-polarization SAR observations exhibit detectable and consistent sensitivity to hydrological transitions under actual field conditions. By linking satellite backscatter dynamics to observed water-level changes, we assess their ability to capture not only the presence or absence of flooding, but also critical transitions in subsurface water status throughout the cropping season. Together, these analyses establish both what constitutes meaningful drainage dynamics in practice and whether such dynamics can be reliably observed from space. This integration is essential for advancing satellite-based monitoring, reporting, and verification (MRV) systems, enabling scalable and independent verification of AWD practices in methane mitigation efforts.

2. Materials and Methods

2.1. Water-Level Observations and Preprocessing

Water-level observations were collected using in situ sensors installed in rice fields, primarily in three study areas: Pangasinan and Cagayan in the Philippines, and Chiba in Japan (Figure 1). These sites were selected to represent regionally important but contrasting rice-growing environments. Pangasinan is a major palay-producing province in the Ilocos Region, with both irrigated and rainfed production and a clear seasonal harvest pattern, whereas Cagayan is located in Cagayan Valley, one of the Philippines' leading rice-producing regions, where palay production is largely supported by irrigated lowland systems and is closely linked to regional water availability [30–32]. Together, the Philippine sites represent tropical, seasonally driven rice systems with two main cropping seasons associated with the wet and dry parts of the year and, in some areas, an intermediate third crop. In contrast, Chiba Prefecture represents a warm-temperate Japanese rice system and a major early-season rice-producing area in the Kanto region, where paddy rice is typically grown as one main spring-to-autumn [33,34]. This site combination allowed us to evaluate sensor-based in situ water-level observations across contrasting agroclimatic settings, rice calendars, irrigation dependence, and rainfall seasonality, from tropical multi-season systems in northern Luzon to a temperate early-season system in Japan.

The raw dataset comprised approximately 2.31 million in situ water-level records collected between 22 January 2024 and 3 March 2026. Because the initial observation period included sensor deployment, testing, and adjustment, records prior to 15 February 2024 were excluded from the analysis. To improve comparability among sensors, water-level measurements were adjusted using sensor-specific correction factors to account for systematic device offsets. The corrected time series were then denoised independently for each sensor using a local outlier filter based on temporally adjacent observations. For each record, neighboring measurements were identified by searching backward and forward in time until the gap between consecutive observations exceeded 30 min, with up to 15 observations retained on each side. Outlier detection was applied only when at least 15 neighboring observations were available in total. The local mean and standard deviation were computed from these neighboring observations, and measurements deviating by more than two standard deviations from the local mean were removed, with the detailed formulation given in Section S1. This procedure was designed to suppress isolated spikes and short-term sensor artifacts

 doi:10.20944/preprints202604.2223.v1

while preserving the broader temporal structure of the water-level series. After these preprocessing steps, observations were assigned to regions based on sensor coordinates, and the final dataset used for drainage-event detection contained 1,988,054 observations from 406 sensors, representing approximately 344 monitored fields across the three study areas.

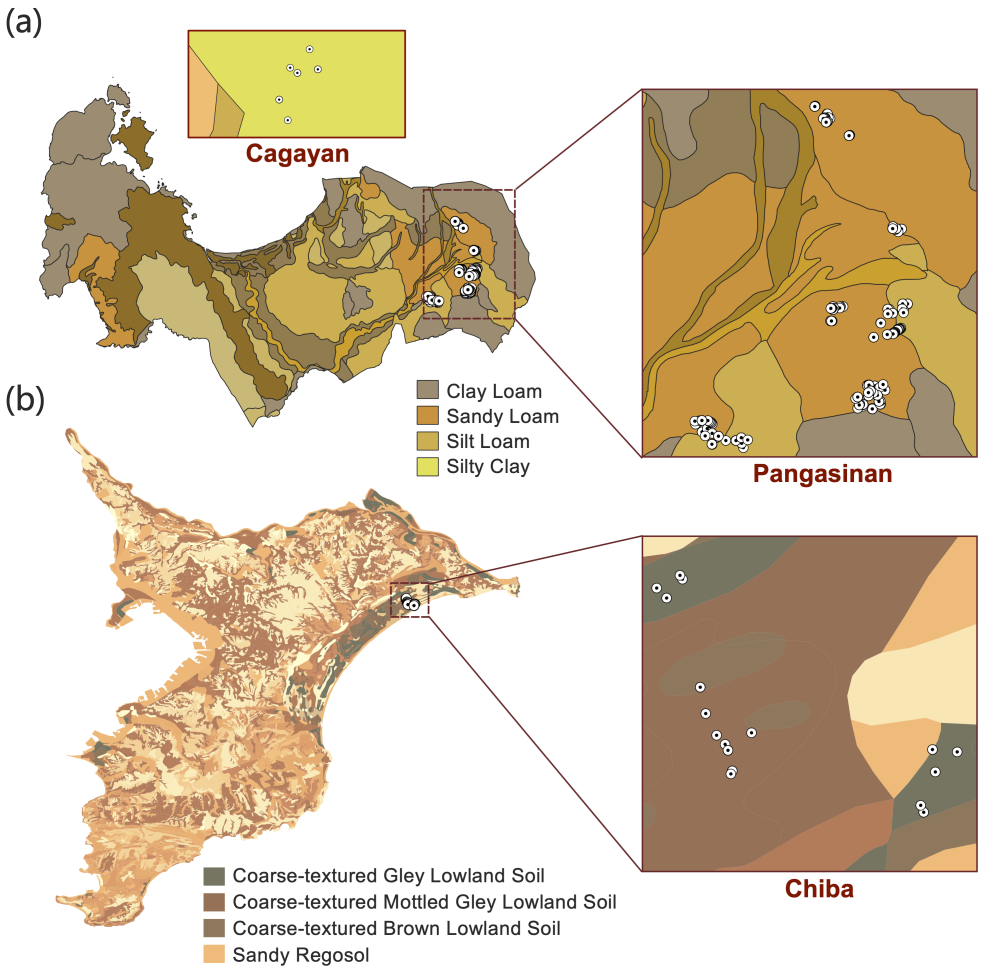

Figure 1. Locations of drainage events and associated soil types in the study regions.

2.2. Drainage Duration Study

2.2.1. Drainage-Event Identification

Drainage events were identified separately for each sensor from the cleaned water-level time series. Conceptually, a drainage event was defined as a sustained recession of water level from a near-surface ponded condition to a drained-condition threshold of -150 mm. Because the exact time at which water level crossed the field-surface reference level, defined as 0 mm, did not necessarily coincide with sensor observation times, event initiation was identified using a near-surface window rather than requiring an observation exactly at 0 mm. Specifically, candidate events were initiated when water level was between 1 and 20 mm above the reference level, thereby capturing the onset of surface-water recession before the water level dropped below the field surface.

After initiation, candidate events were required to satisfy several trajectory-based criteria designed to retain continuous, progressive drainage trajectories while excluding trajectories affected by extended data gaps, short-term noise, or implausible discontinuities. These thresholds were specified as quality-control filters rather than fitted model parameters and were not tuned to maximize the number of detected events. First, the time interval between consecutive observations could not exceed 2 h; longer gaps caused the candidate event to be discarded because the continuity of the drainage trajectory could not be verified across an extended unobserved interval. Second, the water-level trajectory was required

 doi:10.20944/preprints202604.2223.v1

to maintain an overall downward trend, while allowing temporary upward fluctuations of up to 50 mm between consecutive observations. This tolerance was included to accommodate short-term local variability in water level while still requiring a net decline toward the drained threshold. Third, abrupt changes greater than 100 mm between consecutive observations, in either direction, were treated as implausible discontinuities and caused the candidate event to be rejected. This threshold served as a high-magnitude step-change screen to exclude changes inconsistent with progressive drainage. Finally, to confirm that the observed decline represented a progressive drainage process rather than an isolated endpoint crossing, the water level was required to pass through the intermediate range between 0 and -150 mm before reaching the event endpoint.

Because these trajectory-based thresholds could influence whether marginal candidate events were retained or rejected, their robustness was evaluated in the Supplementary Information using a one-at-a-time sensitivity analysis and empirical distributions of consecutive water-level changes (Tables S1 and S2).

This event definition allowed rainfall-related or short-term local fluctuations to be incorporated into a drainage event, provided that the overall drainage trajectory remained intact. However, once water level had dropped below 0 mm, any subsequent rise above 0 mm invalidated the candidate event. In such cases, the preceding decline was not treated as a continuous drainage event, and any later return to near-surface conditions could be evaluated separately as a new candidate event. This rule was used to distinguish within-event fluctuation from the onset of a new surface-water phase.

An event endpoint was assigned when water level reached or fell below -150 mm. The event start time was then refined to the last non-negative observation immediately preceding the accepted decline to the drained threshold, thereby reducing the influence of short plateaus or ambiguous initiation points near the field surface. Thus, the 1–20 mm window was used to identify candidate near-surface conditions, whereas the recorded start time represented the last observed non-negative water level before sustained drainage. For each detected event, start time, end time, start and end water level, duration in hours, and sensor coordinates were recorded. When multiple candidate events shared the same sensor and endpoint, duplicates were removed by retaining the shortest interval.

2.2.2. Duration Metrics, Threshold Comparison, and Variability Analysis

To characterize the observed drainage-duration distribution, event duration was summarized using the median, interquartile range, 90th percentile, and maximum. In addition to these continuous summary statistics, events were grouped into four duration classes: $\leq$ 72 h, 72-168 h, 168-240 h, and $>$ 240 h. These classes were used to examine how drainage events were distributed across progressively longer duration thresholds and to quantify the relative prevalence of rare long-duration events.

For group-based comparison, drainage events were aggregated into four study-defined site–season categories: Chiba, Pangasinan (Wet Season), Pangasinan (Dry Season), and Cagayan (Dry Season). Because the Philippine sites span distinct seasonal cropping periods, events in Pangasinan and Cagayan were classified by season based on both event timing and the actual local rice-cropping conditions observed during field deployment. Events occurring from 1 June to 1 October, which corresponded to the locally observed wet-season rice crop, were assigned to the wet-season group, whereas events from 1 November to 15 April, corresponding to the locally observed dry-season rice crop, were assigned to the dry-season group. These study-defined windows are consistent with the broader Philippine rice calendar and rainfall seasonality: national rice-monitoring frameworks distinguish dry- and wet-season rice semesters, while remote-sensing-based rice-calendar studies show wet-season planting commonly peaking in June–July and dry-season planting in November–December, with substantial regional variation [32,35]. In contrast, the Japanese observations were concentrated within a more limited summer observation window and were therefore treated as a single group rather than subdivided into wet and dry seasons [33,34].

Event duration distributions were compared across these groups using histograms, cumulative distribution functions, and grouped duration-class summaries. For grouped threshold comparison, the

 doi:10.20944/preprints202604.2223.v1

number of events in each duration class was converted to within-group percentages so that the duration composition of each group could be compared on a common 0-100% scale. Spatial distributions of detected events were also summarized to provide site context for the duration comparisons.

To examine variability in drainage patterns across fields, drainage duration was further compared among soil groups and seasonal categories using boxplots on a logarithmic scale. Soil-group differences within each region were assessed using Dunn's nonparametric post hoc test [36] with Holm adjustment [37] for multiple comparisons. Dry–wet contrasts within individual soil groups were evaluated using two-sided Mann–Whitney U tests [38] with Benjamini–Hochberg correction [39] and were applied only where both seasonal groups had sufficient observations in the Philippine sites.

In addition to event duration, field-level recurrence of drainage events was summarized for the Philippine sites by counting the number of detected events per monitored field within each season. Fields were then classified into three categories: no drainage event, single event, and multiple events. This categorization was used to compare how frequently drainage events recurred within the same field under dry- and wet-season conditions.

2.2.3. Explanatory Modeling of Drainage Duration

To explore the factors associated with variation in drainage duration, an explanatory modeling analysis was conducted using event-level predictors representing rainfall input, antecedent wetness, and terrain setting. The purpose of this analysis was not to construct a purely optimized predictive model, but rather to evaluate whether a parsimonious set of physically interpretable variables could explain a substantial share of the observed variation in drainage duration. The final explanatory framework therefore focused on six variables: Accumulated rainfall during the event, mean rainfall intensity during active rainfall periods, antecedent surface soil moisture, antecedent root-zone soil moisture, elevation, and slope.

Geospatial extraction was implemented in Google Earth Engine [40]. Rainfall-related variables were derived for each drainage event from the GSMaP V7 operational hourly precipitation product, using the Earth Engine collection `JAXA/GPM_L3/GSMaP/v7/operational` and the `hourlyPrecipRate` band at the sensor location [41–44]. For each event, hourly precipitation was extracted from event start to event end, and accumulated rainfall was calculated as the cumulative precipitation over the event duration. Mean rainfall intensity was calculated as the mean hourly precipitation considering only hours with rainfall greater than 0.001 mm h^{-1}. Antecedent wetness conditions were represented using surface soil moisture and root-zone soil moisture derived from the SMAP L4 3-hourly 9-km soil-moisture product, using the Earth Engine collection `NASA/SMAP/SPL4SMGP/008`. The extracted variables were `sm_surface`, representing near-surface soil moisture for the 0–5 cm layer, and `sm_rootzone`, representing root-zone soil moisture for the 0–100 cm layer [45,46]. For each drainage event, the latest available SMAP L4 observation within the 24 h preceding event start was extracted at the sensor location. Elevation was extracted from the NASA Shuttle Radar Topography Mission 30 m digital elevation model, using the Earth Engine image `USGS/SRTMGL1_003` [47]. Slope was derived from the same DEM using `ee.Terrain.products` and was sampled at each sensor location. The explanatory variables included in the final analysis are summarized in Table 1.

The response variable was drainage duration in hours. Model training was conducted using a LightGBM regressor, a gradient-boosted decision-tree method based on the gradient boosting framework [48] and designed for efficient supervised learning with tabular data [49]. The dataset was divided into training and testing subsets, and model performance was evaluated on held-out test data using R^2, root mean square error (RMSE), and mean absolute error (MAE). RMSE and MAE were both reported because they summarize complementary aspects of prediction error magnitude [50,51]. To interpret the fitted model, variable importance rankings and SHAP (Shapley Additive Explanations) values were examined [52]. Because the fitted model was a tree ensemble, SHAP-based feature attributions were interpreted in the TreeSHAP framework [53]. SHAP values were used to quantify the contribution of each predictor to the model output and to evaluate how individual variables were associated with longer or shorter predicted drainage duration.

 doi:10.20944/preprints202604.2223.v1

Potentially important controls related to field management and crop phenology were not included in the final explanatory analysis. In rice systems, irrigation scheduling, drainage operation, and crop growth stage are all likely to affect drainage duration. However, these variables were not available in a sufficiently consistent and accurate form across all monitored fields. The final model should therefore be interpreted as a hydrology- and terrain-based explanatory analysis rather than a complete representation of all determinants of drainage duration.

Table 1. Variables used in the explanatory modeling analysis of drainage duration.

Variable	Dataset	Spatial resolution	Temporal resolution	Extraction method	Notes
Antecedent surface soil moisture (`sm_surface_before`)	SMAP L4	~9 km	3-hourly	Latest pre-event SMAP observation within 24 h at the sensor location.	Unit: m^3/m^3; near-surface layer (0–5 cm).
Antecedent root-zone soil moisture(`sm_rootzone_before`)	SMAP L4	~9 km	3-hourly	Latest pre-event analysis estimate within 24 h at the sensor location.	Unit: m^3/m^3; root-zone layer (0–100 cm).
Accumulated rainfall during the event (`rainfall_total_mm`)	GSMaP V7	~0.1° (~10 km)	Hourly	Hourly rainfall extracted over the event period and summed.	Unit: mm.
Mean rainfall intensity during rainy hours (`rainfall_active_mean_intensity`)	GSMaP V7	~0.1° (~10 km)	Hourly	Mean hourly rainfall over the event period using only hours with rainfall > 0.001 mm h^{-1}.	Unit: mm h^{-1}.
Elevation (`elevation`)	SRTM DEM	30 m	Static	Elevation sampled at each sensor location.	Unit: m above sea level.
Slope (`slope`)	Slope from SRTM DEM	30 m	Static	Computed from the DEM and sampled at each sensor location.	Unit: degrees.

2.3. Remote Sensing Study

2.3.1. PALSAR-2 Observations

L-band Synthetic Aperture Radar (SAR) inherits advantages in monitoring hydrological condition in paddy fields due to its deeper penetration through the paddy canopy. Observations from Phased Array type L-band SAR 2 (PALSAR-2) onboard the Advanced Land Observing Satellite 2 (ALOS-2) operated by the Japan Aerospace Exploration Agency (JAXA) were utilized for this study. Specifically, the open-access Level 2.2 (L2.2) ScanSAR product was used, which contains dual-polarization backscatter in HH and HV, local incidence angle (LIN) and quality flag (MSK) at a spatial resolution of 25 m and a swath width of 350 km. The L2.2 product is ortho-rectified, radiometrically terrain-corrected, and normalized to gamma naught (γ^0), making it compatible with the Committee on Earth Observation Satellites (CEOS) Analysis Ready Data for Land (CARD4L) standard [54]. The L-band microwave frequency (1.27 GHz, 23.6 cm wavelength) provides deep canopy penetration relative to the C-band sensors, allowing detection of soil surface and even sub-surface water conditions below the rice canopy throughout the growing season [21,26].

The PALSAR-2 L2.2 ScanSAR images were accessed and processed using the Google Earth Engine (GEE) platform with the snippet `JAXA/ALOS/PALSAR-2/Level2_2/ScanSAR`. The data set did not contain scenes that cover the paddy fields in Japan. Therefore, this study was limited to paddy fields in the Philippines and those cultivated from the wet cropping season of 2024 to the wet cropping season of 2025. PALSAR-2 data were retrieved from June 2024 to October 2025 for the paddy fields in the Pangasinan region introduced in 2.1. A summary of the frames retrieved are given in Table 2 with spatial extents and temporal distribution, respectively, shown in Figure 2 and Figure 3. Details of each scene are given in Table S5.

 doi:10.20944/preprints202604.2223.v1

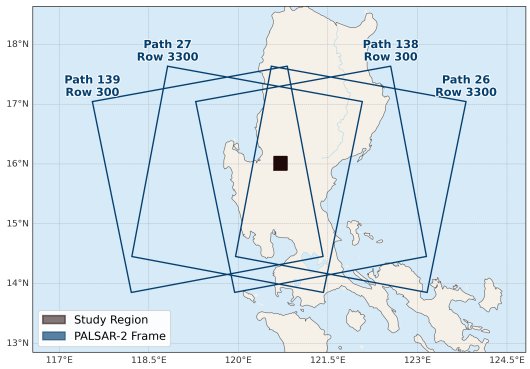

Figure 2. Spatial extent of the retrieved PALSAR-2 L2.2 ScanSAR frames.

Table 2. Summary of the retrieved PALSAR-2 L2.2 ScanSAR scenes.

Path Number	Row Number	Orbit Direction	Antenna Direction	Number of scenes
26	3300	Descending	Right	3
27	3300	Descending	Right	4
138	0300	Ascending	Right	7
139	0300	Ascending	Right	17

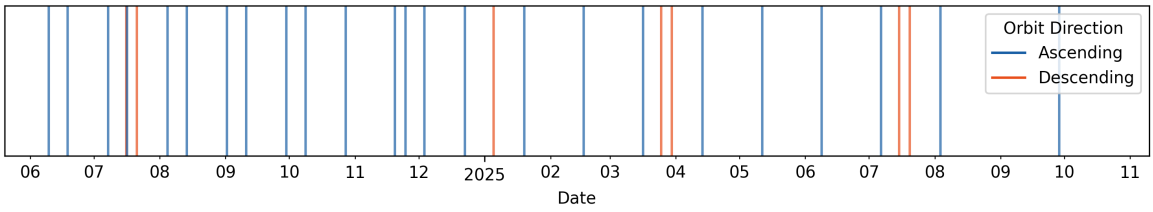

Figure 3. Temporal distribution of retrieved PALSAR-2 L2.2 ScanSAR scenes.

The HH and HV bands of each scene were processed by, first masking with the MSK-band to retain valid pixels with the MSK value of 1, and then converting the data in digital number (DN) to decibels (dB) using Equation 1 [54]. Finally, the median HH and HV backscatter values of each paddy field were calculated as the representative backscatter signal of the field. Additionally, HH/HV ratio was calculated using Equation 2. The processed data set contains paddy field name, observation time, HH backscatter, HV backscatter, and HH/HV ratio.

$$\gamma^0(dB) = 10 \cdot \log_{10}(DN^2) - 83.0 \tag{1}$$

$$Ratio_{HH/HV}(dB) = \gamma^0_{HH}(dB) - \gamma^0_{HV}(dB) \tag{2}$$

2.3.2. Derivation of Crop Stage from Water Level Observations

Field-scale water level readings observed at 15 minute intervals were preprocessed in Section 2.1, and the resulting data set contains the time series of water level readings of each paddy field. The water level sensors were installed in the field just after planting the paddy and removed just before harvest. Therefore, the readings are available only from the tillering stage to the maturity stage of the paddy phenology. It was noted that, the monitored paddy fields followed different farming practices in terms of planting method (direct seeding and transplanting), planting date, irrigation, and harvesting date. Consequently, the growth stage on a given day varies across fields. Since, SAR scattering mechanism varies with paddy phenology, it is important to identify the field-scale season and the growth stage.

We utilized the water level readings itself to derive the respective cropping seasons (hereafter referred season) and the growth stage for each reading. In Pangasinan region, paddy is cultivated

 doi:10.20944/preprints202604.2223.v1

in three cropping seasons namely, Dry (planting from October to December of the previous year), Third (planting from February to April), and Wet (planting from June to August). The water level observations did not contain records from harvesting to planting of the net season. Leveraging this temporal gap in the time series, first, water level time series of each field were segmented in to seasons adopting a minimum of 21 day time gap between consecutive water level readings. The start of each season is identified as the sensor installation date and the end as the sensor decommissioning date (A sample segmented time series is shown in Figure S3. Segmented seasons were labeled Wet-, Dry- or Third-season depending on their start date being in the respective planting period. Considering a usual 60 to 180 day season duration, the segmented seasons were filtered for ones eligible for further analysis. The distribution of the resulting field-scale season durations are shown in Figure 4. Due to the significant variability in field-scale season durations Figure S4, and varying farming practices, instead of the commonly used 'number of days from sowing' [21], a dynamic growth stage definition based on the progress in the season was adopted. Accordingly, three growth stages namely Early, Mid and Late were defined bounded by 0, 30, 70, and 100% of field-scale season progress, based on the L-band HH behavior published by [23]. An illustration for the derivation of the bounds is shown in Figure S5.

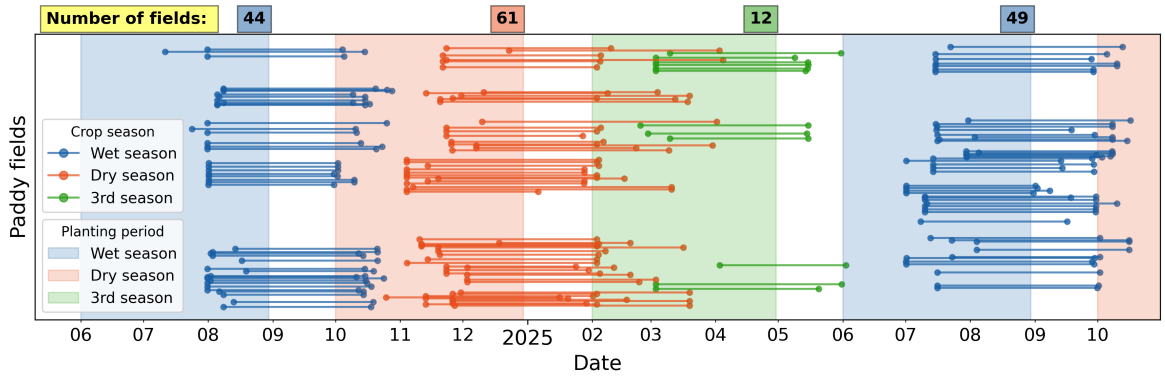

Figure 4. Identified field-scale crop seasons. Start and end dates of the seasons correspond to sensor installation and decommissioning dates.

The dual polarization radar backscatter signals are sensitive to inundation and structural development of the canopy in paddy fields. In the presence of standing water, both HH and HV signals tend to be minimal during the early growth stage due to specular scattering, then increase with time due to double bounce from growing stems and volume scattering from the canopy [23,25]. The absence of water increases HH due to increased single/surface scattering in the early stage, and reduces due to reduced double bounce scattering in later stages. And HV remains unchanged as volume scattering remains constant regardless of the inundation condition [21]. The corresponding rice phenology for crop stage classes and the expected dual polarized backscatter behavior is stated in Table 3. The processed data set contains paddy field name, observation time, water level, corresponding season and growth stage.

 doi:10.20944/preprints202604.2223.v1

Table 3. Defined growth stages and the corresponding paddy phenology and, expected HH and HV variations.

Growth stage	Season progress (%)	HH [Inundated]	HV [Inundated]	Paddy phenology stages
Early	0 - 30	Low [Very low]	Low [Very low]	Tillering
Mid	30 - 70	Low [Medium]	Low [Low]	Stem elongation, Panicle initiation, Booting, Heading, Flowering
Late	70 - 100	Medium [High]	Medium [Medium]	Milk, Dough, Mature

2.3.3. Pairing PALSAR-2 and In Situ Water Level Observations

For direct comparison between field-scale SAR backscatter and hydrological conditions, each PALSAR-2 observation was paired with an in situ water level observation from the same field, observed within 10 minutes from the PALSAR-2 observation time. This narrow window was adopted to minimize the misrepresentation of field conditions in case of rapid water level fluctuations such as from rainfall, irrigation, or drainage events that could introduce mismatches between the SAR signal and the actual ground conditions at the overpass time. Furthermore, it was noted that the PALSAR-2 L2.2 ScanSAR scene `ALOS2554990300-240901_WBDR1.1__A` (observed on 1 September 2024) contained strip noise Figure S2, and the related observations were omitted from the analysis and the distribution of omitted samples are marked in red color in the Figure 5. The processed data set contained 400 records with information of field identity, PALSAR-2 observation time, HH backscatter, HV backscatter, HH/HV ratio, water level, season, and growth stage.

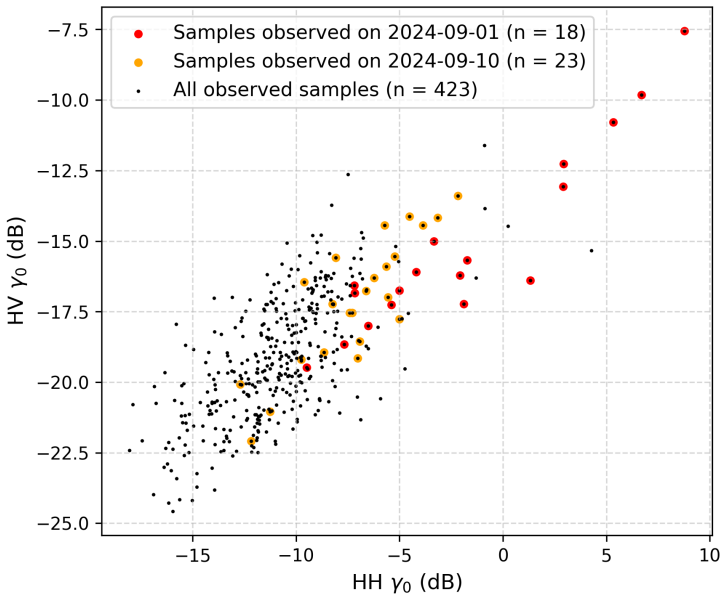

Figure 5. The distribution of paired samples in HV vs HH space. Samples marked in red were removed due to strip noise (observed on 1 September 2024). The sampled marked in orange were removed in later stage of analysis due to suspected overestimated SAR observation (observed on 10 September 2024).

2.3.4. Statistical Significance Test

To evaluate whether the PALSAR-2 backscatter signals differ significantly between the inundation condition classes, independent samples t-tests were conducted for each crop stage category and for the combined all-stages data set. The t-test was selected as an appropriate parametric test for comparing the means of two independent groups, given that the inundation condition within each crop stage

 doi:10.20944/preprints202604.2223.v1

constitute independent samples drawn from distinct field-level water conditions. In cases where only a single sample was available in one of the inundation classes, an independent samples t-test could not be computed due to insufficient degrees of freedom. For these instances, a one-sample t-test was applied instead. While this approach carries greater uncertainty than a standard t-test owing to the absence of variance information from the single-sample class, it was adopted as a solution to provide complete statistical analysis. Results from one-sample t-tests are reported alongside their counterparts but should be interpreted with appropriate caution. All statistical analyses were conducted in Python using the SciPy library (scipy.stats.ttest_ind, and scipy.stats.ttest_1samp for the one-sample cases).

3. Results

3.1. Drainage Duration Study

3.1.1. Distribution of Drainage Event Duration

Identified drainage events were distributed across the monitored sites in Pangasinan, Cagayan, and Chiba, spanning several contrasting soil environments (Figure 1). A total of 564 drainage events were identified from the water-level observations, with examples shown in Figure 6. Across all events, the median drainage duration was 19.0 h, with an interquartile range of 8.2-42.1 h, a 90th percentile of 79.0 h, and a maximum observed duration of 336.8 h (Table 4). The overall distribution was strongly right-skewed, with most events concentrated at short durations and only a small number extending into the long-duration tail (Figure 7).

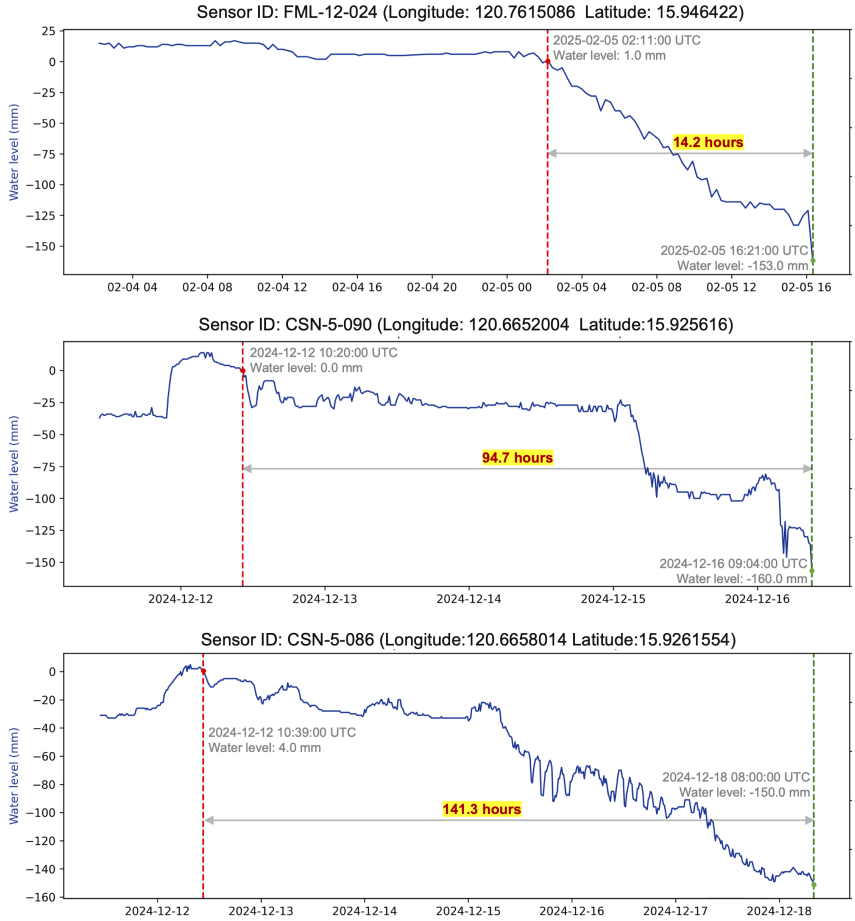

Figure 6. Examples of detected drainage events from water-level time series across different sensors. Each event is identified as a sustained decline from near-surface conditions to the drainage threshold. The red dashed line marks the event start, and the green dashed line marks the event end.

Clear regional differences were signifiacant in both the histogram and cumulative distribution (Figure 7). Pangasinan was dominated by shorter drainage events, especially during the wet season.

 doi:10.20944/preprints202604.2223.v1

The median duration was 10.6 h in Pangasinan (Wet season) and 21.4 h in Pangasinan (Dry season). In contrast, drainage events in Chiba and Cagayan were substantially longer. Chiba had a median duration of 53.5 h, whereas Cagayan (Dry Season) showed the longest duration profile, with a median of 72.6 h and a 90th percentile of 280.3 h (Table 4).

To assess how drainage duration was distributed across progressively longer timescales, we examined four duration classes: $\leq$ 72 h, 72–168 h, 168–240 h, and $>$ 240 h. Overall, only 5 of 564 events (0.9%) lasted longer than 240 h (Table 4). Most events fell within the shortest duration class ($\leq$ 72 h), especially in Pangasinan, where 92.8% of wet-season events and 89.8% of dry-season events were shorter than 72 h (Figure 8). In contrast, Chiba and Cagayan contained a larger proportion of longer-duration events. In Chiba, 24.0% of events fell within the 72–168 h class, 12.0% within the 168–240 h class, and 4.0% exceeded 240 h. Cagayan (Dry season) showed the highest share of long-duration events, with 36.4% in the 72–168 h class and 18.2% exceeding 240 h.

Taken together, these results indicate that observed drainage durations were generally much shorter than 240 h, although substantial regional differences were evident. Long-duration drainage events were uncommon overall, but they occurred more frequently in Cagayan and, to a lesser extent, in Chiba than in Pangasinan. However, these regional comparisons should be interpreted with caution, particularly for Cagayan, because the number of detected events was limited in both Chiba ($n = 25$) and Cagayan ($n = 11$).

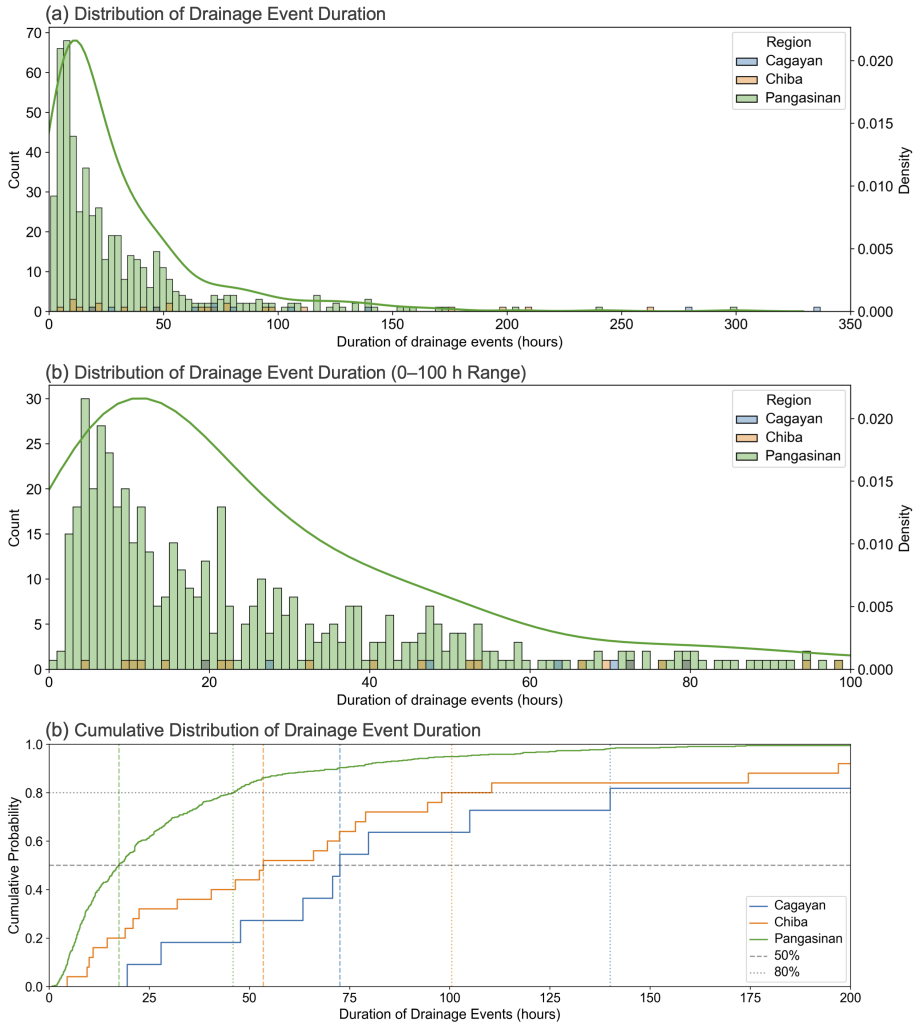

Figure 7. Frequency and cumulative distributions of drainage event duration across regions: (a) full distribution of event duration, (b) zoomed-in view of the 0–100 h range from panel (a), and (c) cumulative distribution function of drainage event duration.

 doi:10.20944/preprints202604.2223.v1

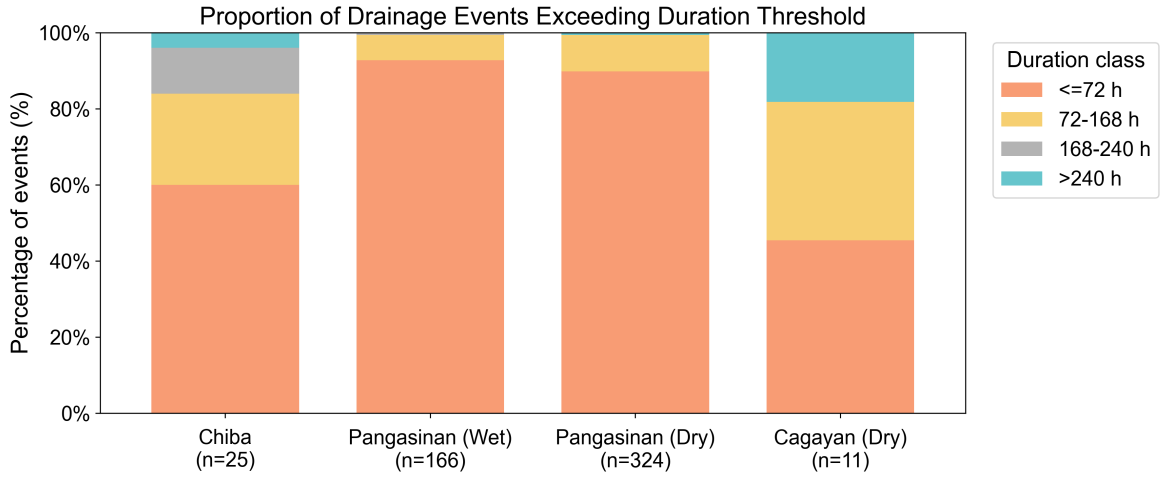

Figure 8. Proportional distribution of drainage event duration classes across regions and seasons, expressed as percentages of total events.

Table 4. Summary of drainage duration statistics.

Group	n	Median (h)	Q1–Q3 (h)	P90 (h)	Max (h)	Events >240 h, n (%)
Overall	564	19.0	8.2–42.1	79.0	336.8	5 (0.9%)
Chiba	25	53.5	21.0–94.5	188.0	263.5	1 (4.0%)
Pangasinan (Wet)	166	10.6	6.3–24.1	51.6	171.3	0 (0.0%)
Pangasinan (Dry)	324	21.4	9.8–42.1	72.3	299.3	2 (0.6%)
Cagayan (Dry)	11	72.6	55.6–122.5	280.3	336.8	2 (18.2%)

3.1.2. Variability in Drainage Event Duration Across Fields

Substantial heterogeneity in drainage patterns was observed across soil environments and fields. The detected drainage events were associated with distinct soil groups in the three study regions (Figure 9). In Cagayan, all detected events occurred in Silty Clay soils. In Chiba, detected events were distributed across three mapped lowland soil groups, including Brown Lowland Soil, Gley Soil, and Mottled Gley Soil. In Pangasinan, most detected events were associated with Sandy Loam ($n = 428$) and Silt Loam ($n = 95$), indicating that variability in drainage behavior was concentrated within these dominant soil environments.

Drainage duration also differed across soil groups (Figure 9). In Cagayan, the Silty Clay fields showed relatively long drainage durations, with a median of 72.6 h. In Chiba, median drainage duration varied among the three soil groups, ranging from 47.0 h in Gley Soil to 69.5 h in Mottled Gley Soil. In Pangasinan, median durations were substantially shorter, at 17.5 h for Sandy Loam and 17.5 h for Silt Loam. These results indicate that the duration of drainage events varied not only across regions, but also across the soil environments in which the monitored fields were located.

Seasonal contrasts were most evident in Pangasinan (Figure 10). In Sandy Loam fields, drainage duration was significantly longer in the dry season than in the wet season, with median values of 21.4 h and 9.9 h, respectively ($p < 0.001$). In Silt Loam fields, drainage duration also tended to be longer in the dry season than in the wet season (21.6 h vs. 12.5 h), although this difference was not statistically significant after multiple-comparison correction. In Cagayan, only dry-season events were available, and therefore no dry–wet comparison could be performed.

Field-level recurrence patterns further highlighted seasonal heterogeneity (Table 5). Across the Philippine sites, 48.0% of fields experienced multiple drainage events during the dry season, compared with only 21.6% in the wet season. Conversely, the proportion of fields with no detected drainage event increased from 22.3% in the dry season to 60.8% in the wet season. This indicates that, even when drainage duration may be broadly comparable within some soil groups, the recurrence of drainage events within the same field was substantially higher in the dry season than in the wet season.

 doi:10.20944/preprints202604.2223.v1

Taken together, these results demonstrate that drainage patterns were highly variable across fields, reflecting both spatial heterogeneity among soil environments and seasonal differences in field-level drainage activity. In particular, the Pangasinan sites showed clear seasonal differences not only in event duration, but also in the frequency with which drainage events recurred within the same field.

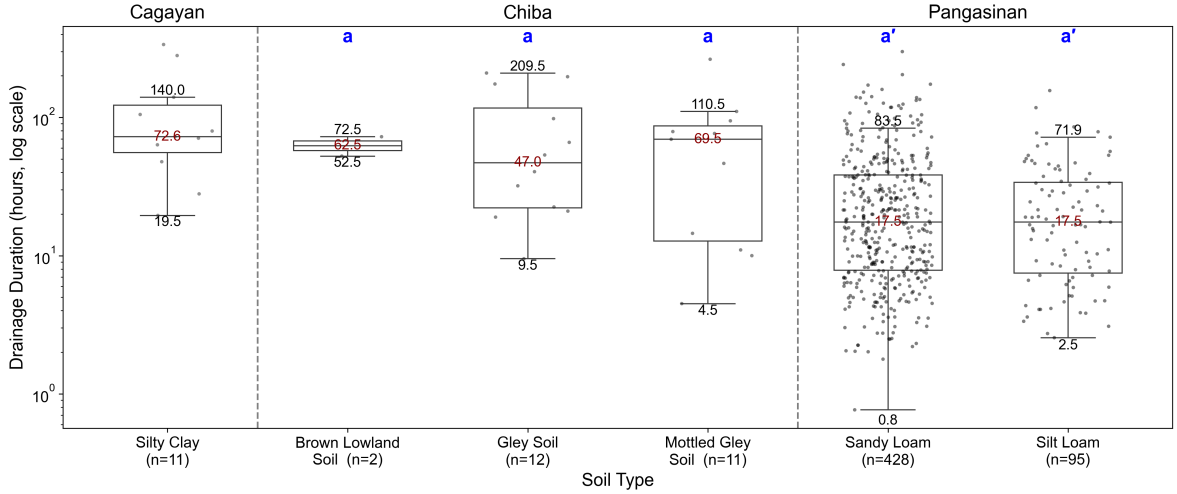

Figure 9. Distribution of drainage event duration across soil types and regions. Boxplots (log scale) illustrate variability in event duration for each soil type within Cagayan, Chiba, and Pangasinan. Different letters indicate statistically significant differences between soil types within each region.

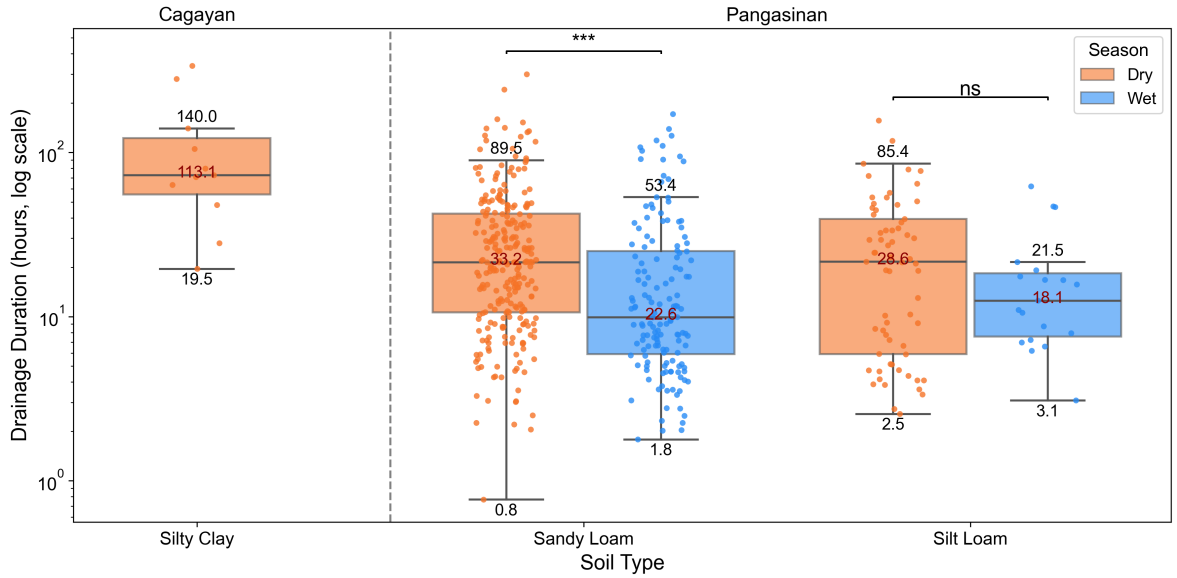

Figure 10. Comparison of drainage event duration between dry and wet seasons across soil types and regions. Boxplots (log scale) illustrate seasonal differences in event duration for each soil type. Statistical significance is indicated as follows: *** $p < 0.001$, * $p < 0.05$, ns: not significant.

Table 5. Number of Philippine fields with no, single, or multiple drainage events by season.

Category	Dry, n (%)	Wet, n (%)
No drainage event	33 (22.3%)	90 (60.8%)
Single event	44 (29.7%)	26 (17.6%)
Multiple events	71 (48.0%)	32 (21.6%)

 doi:10.20944/preprints202604.2223.v1

3.2. *Remote Sensing Study*

3.2.1. Backscatter Variability with Vertical Water Distribution

To explore the relationship between L-band SAR backscatter and field-scale water conditions, the backscatter values of HH and HV polarizations and and the HH/HV ratio were plotted against coincident in situ water level observations, as shown in Figure 11a. The plots reveal a clear but non-uniform structure in the dual-polarization backscatter and water level relationship across the observed range (+100 to -200 mm), with a notable zone of high signal variability concentrated in the intermediate water level range of approximately +40 to -110 mm. This range is defined as the semi-inundation zone, representing the transition between full- and non-inundation conditions. Correspondingly, full-inundation refers to water level observations above +40 mm and non-inundation to water levels below -110 mm. In the field, semi-inundated conditions are characterized by spatially intermittent ponding and moist soil attributable to micro-topographic variability within the paddy fields (Figure 12), where a mix of scattering mechanisms occur. According to Figure 11a, anomalously high backscatter signals in both HH and HV are observed in the semi-inundated fields (marked with a red rectangle). Although these anomalous values predominantly falls within the semi-inundated range, consistent with field-scale water level conditions, the corresponding samples were originating from a signal PALSAR-2 L2.2 ScanSAR scene `ALOS2556320300-240910_WBDR1.1__A` observed on 10 September 2024 (also shown in Figure 5). As these anomalies are likely attributable to a scene-level acquisition or processing artifact, the samples acquired on 10 September 2024 were excluded from further analysis, and the updated scatter plots are shown in Figure 11b.

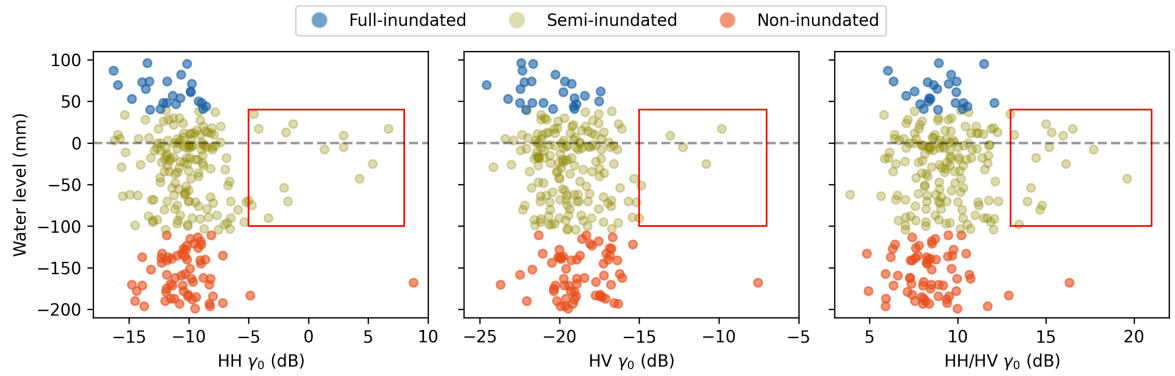

(**a**)

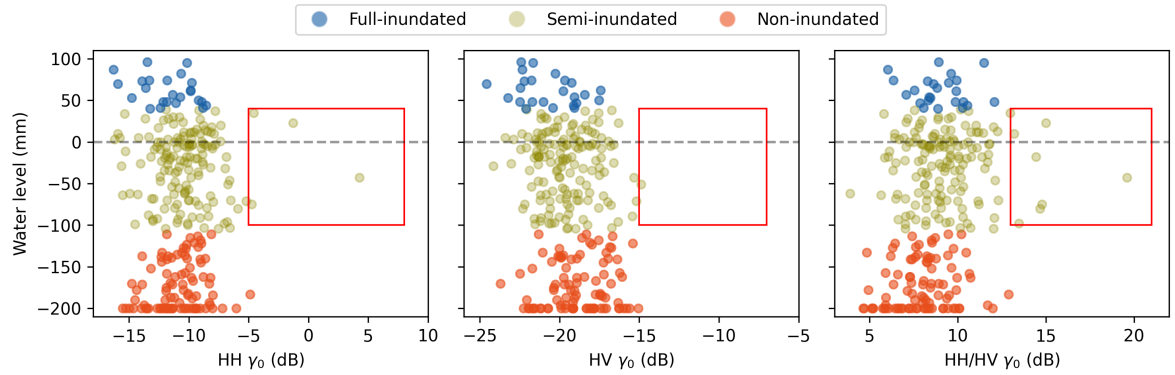

(**b**)

Figure 11. Scatter plots of water level vs backscatter HH, HV and HH/HV ratio. (**a**) All observations. (**a**) Excluding observations on 10 September 2024. The extreme observations are marked with a red rectangle.

 doi:10.20944/preprints202604.2223.v1

(**a**) (**b**)

Figure 12. Paddy field images showcasing semi-inundated conditions. (**a**) Field overview. (**b**) Close-up look.

3.2.2. Distinguishing the Field Inundation Condition

Figure 13 presents the relationship between backscatter signals (in HV vs HH space) and inundation status across different crop growth stages. Across all stages, a clear positive correlation is observed between HH and HV polarizations. This relationship is most pronounced during the Late growth stage, where the data exhibit a tighter spread along a linear trend, suggesting a more consistent canopy structure and scattering response from mature paddy plants, and minimal influence from the inundation condition. In contrast, the Early and Mid growth stages show greater dispersion, likely reflecting higher variability in early establishment conditions where remote sensing is open for direct surface observation of varying inundation conditions and rapidly varying paddy plant structure, than in the Late growth stage where structurally homogeneous thick crop canopy covers the surface.

Despite the overall correlation, the three inundation classes (full-, semi-, and non-inundated) show substantial overlap in the HV vs HH feature space across all growth stages. This overlap is particularly evident when all stages are combined, where class boundaries become indistinct. While minor tendencies can be observed—such as slightly lower HV backscatter values under full-inundated conditions, the separation is not sufficiently distinct to allow reliable discrimination using HH and HV alone, across growth stages.

A statistical analysis was conducted to evaluate the distinguishability between full- and non-inundated classes across different growth stages (Early, Mid, and Late) by comparing the distributions of HH and HV backscatter, as well as the HH/HV ratio (Figure 14). Statistical significance between full-inundated and non-inundated categories was assessed using an independent samples t-test. In cases where only a single sample was available within a dataset, a one-sample t-test was applied; however, such comparisons should be interpreted with caution due to limited sample representation. In general, fully inundated conditions were associated with lower backscatter values (HH and HV). This observation is theoretically consistent during the Early growth stage, where specular reflection from the water surface leads to reduced backscatter. However, during the Late growth stage, increased double-bounce scattering between rice stems and the water surface would be expected to enhance HH backscatter. The observed deviation from this expectation may be attributed to the limited sample size, particularly the presence of only a single sample in this category. HV backscatter exhibited a more consistent trend, with increasing backscatter corresponding to decreasing water levels. Statistically significant differences at the 95% confidence level were observed during the Mid growth stage. In contrast, the HH/HV ratio (Figure 14(**c**)) showed broadly similar median values across inundation classes, indicating no statistically significant separation between full- and non-inundated conditions at these stages. However, when considering the entire season, the distributions indicate a systematic yet strongly overlapping variation in SAR backscatter between full- and non-inundated classes. Although HV backscatter and the HH/HV ratio exhibit statistically significant differences, suggesting some

 doi:10.20944/preprints202604.2223.v1

potential for distinguishing inundation conditions, the substantial overlap among the classes limits their reliability as standalone indicators of inundation.

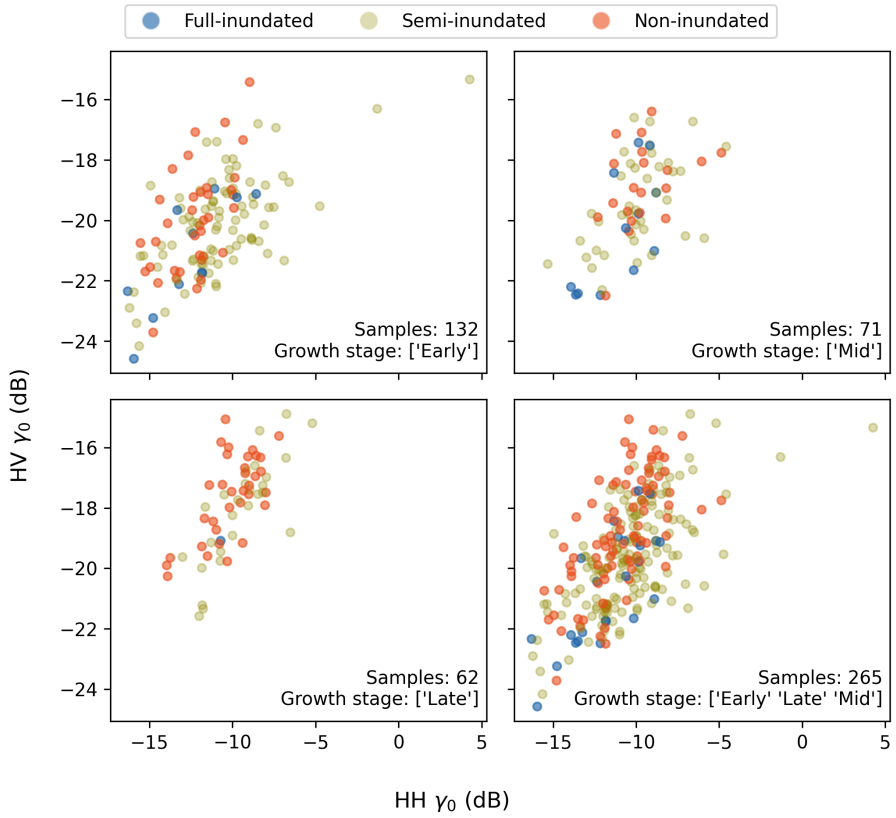

Figure 13. Scatter plots of samples in HV vs HH space for each crop stage and all stages combined together.

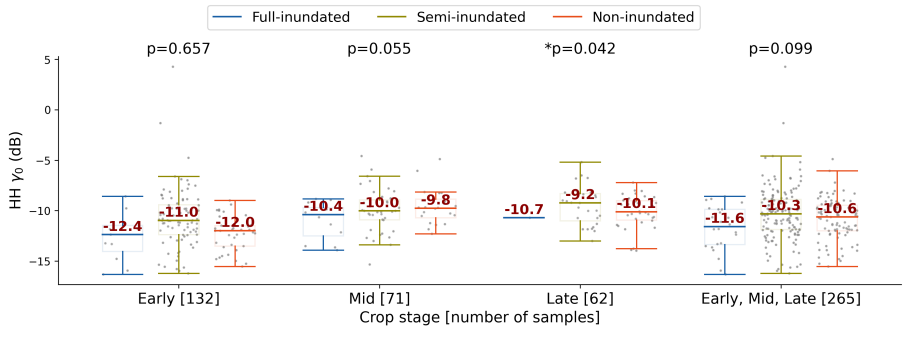

(**a**)

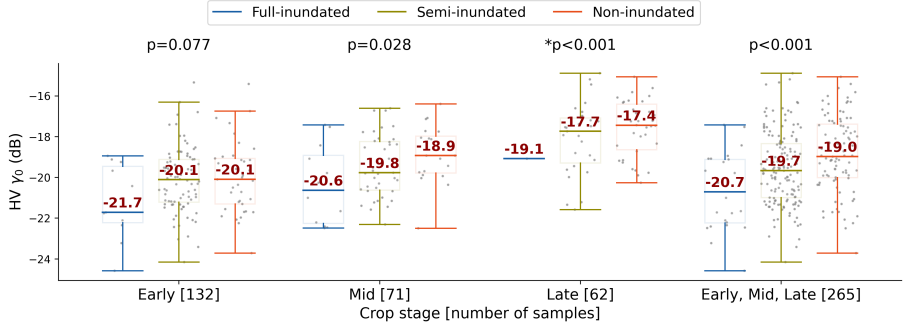

(**b**)

Figure 14. *Cont.*

 doi:10.20944/preprints202604.2223.v1

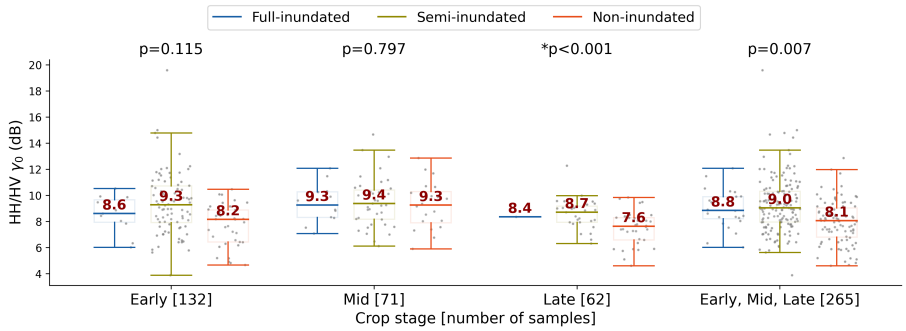

(**c**)

Figure 14. Backscatter variability with crop stage and inundation conditions for (**a**) HH. (**b**) HV. (**c**) HH/HV. The median values related to each box plot is shown in red. The p-value for the t-test between full- and non-inundated classes is show above the corresponding crop stage. An '*' indicates the use of one-sample t-test.

4. Discussion

4.1. Observed Drainage Duration and Variability

The observed drainage events were generally short relative to 240 h, with only a small fraction extending beyond this duration. Across all identified events, the median drainage duration was 19.0 h, and only 5 of 564 events (0.9%) exceeded 240 h (10 days)(Figure S1). This indicates that, under the monitored field conditions represented in this study, prolonged drainage events were uncommon and that most fields reached drained conditions within a much shorter time frame. In this sense, the observed duration distribution was strongly concentrated at the short-duration end, with only a limited long-duration tail.

At the same time, drainage duration varied substantially across regions and seasons. Pangasinan was dominated by shorter events, particularly during the wet season, whereas Chiba and Cagayan showed longer duration profiles. Cagayan (Dry Season) exhibited the largest proportion of long-duration events, although this result should be interpreted cautiously given the limited sample size.

These regional contrasts suggest that drainage duration is not characterized by a single common timescale, but instead reflects differences in hydrologic setting (e.g., ponding depressions, ditch-connected plots; [55,56]), field conditions (e.g., sandy loam, raised bunds; [57,58]), and seasonal context (e.g., dry-season drawdown, wet-season rainfall; [10,59]) among the monitored systems.

These regional contrasts suggest that drainage duration is not characterized by a single common timescale, but instead reflects differences in hydrologic setting, field conditions, and seasonal context among the monitored systems.

Seasonal variability was especially evident in Pangasinan, where drainage duration in Sandy Loam fields was significantly longer in the dry season than in the wet season, while the same tendency was present but not statistically significant in Silt Loam. At first glance, this pattern may seem counter-intuitive, because wetter antecedent conditions would generally be expected to impede drawdown. However, in managed rice fields, drainage duration is likely shaped not only by antecedent wetness, but also by irrigation scheduling, drainage operations, and the overall timing of field water management. One plausible interpretation, consistent with the patterns shown in subsubsection 3.1.2, is that dry-season events more often reflect deliberate and sustained field drainage under active water control, whereas wet-season water-level changes may be more fragmented or irregular due to frequent rainfall input. This interpretation is consistent with studies of irrigated lowland rice showing that AWD and related controlled-irrigation practices deliberately allow fields to drain or become non-flooded before re-irrigation [60,61]. In contrast, wet-season water-level changes may be more fragmented or irregular because frequent rainfall and excess-water removal can repeatedly interrupt drawdown in humid tropical rice systems [62,63].

This interpretation is broadly consistent with the field-level recurrence analysis, which showed that multiple drainage events within the same field were much more common in the dry season than

 doi:10.20944/preprints202604.2223.v1

in the wet season. Together, these results suggest that dry-season drainage in Pangasinan may be characterized by more frequent and more sustained management-driven drainage activity, while wet-season water-level dynamics may be less likely to produce long, continuous drainage episodes. The lack of a statistically significant dry–wet contrast in Silt Loam does not necessarily indicate the absence of a seasonal effect, but may instead reflect greater within-group variability and the smaller number of wet-season observations in that soil class.

Another important aspect of variability was the recurrence of drainage events within the same field. Nearly half of the monitored Philippine fields experienced multiple drainage events during the dry season, whereas this proportion was much lower in the wet season, when most fields showed no detected drainage event. This indicates that seasonal differences were expressed not only in the duration of individual events, but also in how frequently drainage events recurred within the same field. Together, these results suggest that drainage behavior in rice systems is highly heterogeneous, varying across regions, seasons, and field contexts rather than following a uniform pattern.

Notably, soil-group contrasts within individual regions were less pronounced than the broader regional and seasonal differences. Although drainage duration varied among soil classes, these within-region soil contrasts were not statistically significant in the present dataset. This suggests that, at least in the monitored fields considered here, regional setting and seasonal conditions may have exerted a stronger influence on drainage behavior than soil-group differences alone, or that potential soil effects were masked by substantial field-level heterogeneity and unobserved management variation.

4.2. Interpretable Factors Associated with Drainage Duration

To complement the descriptive analyses above, we fitted a parsimonious and physically interpretable random-forest regression model using six variables representing rainfall input, antecedent wetness, and terrain setting. The model was intended primarily for model-based interpretation rather than for optimized prediction. It nevertheless retained moderate out-of-sample performance, with a test R^2 of 0.492, RMSE of 31.32 h, and MAE of 19.87 h. These results suggest that the selected environmental predictors contained substantial information on drainage duration in the held-out data. However, the MAE was comparable to the median observed drainage duration reported above, indicating that the model should be viewed as more useful for identifying broad environmental associations than for precise event-level prediction. In addition, because some fields contributed multiple drainage events, event-level data splitting may not fully evaluate generalization to entirely unseen fields or regions. The model results should therefore be interpreted as evidence of associations within the fitted dataset, rather than as a complete or fully transferable predictive explanation of drainage duration.

At the same time, nearly half of the variation remained unexplained, which is expected in managed rice systems. Drainage duration is influenced by a range of site-specific factors not captured by the explanatory variables, including irrigation scheduling, deliberate drainage operations, bund and outlet management, and crop growth stage, as well as local hydraulic connectivity that varies at fine spatial scales. Thus, rainfall input, antecedent water storage, and field setting together provided meaningful but incomplete information on how long drainage persisted.

Interpreted as model-based predictive importance, the SHAP ranking (Figure 15) indicates that accumulated rainfall during the event was the most influential variable among the six selected environmental predictors, followed by mean rainfall intensity during rainy hours, elevation, and antecedent root-zone soil moisture. Among these, the most physically interpretable and internally consistent signals were associated with accumulated rainfall and antecedent root-zone wetness. Greater rainfall accumulation during the event tended to increase predicted drainage duration, which is consistent with the expectation that larger water inputs prolong the time required for fields to reach drained conditions [64,65]. However, accumulated rainfall during the event should be interpreted as an event-scale co-occurring water-input metric rather than as a strictly antecedent predictor, because longer drainage events also provide a longer window over which rainfall can accumulate.

 doi:10.20944/preprints202604.2223.v1

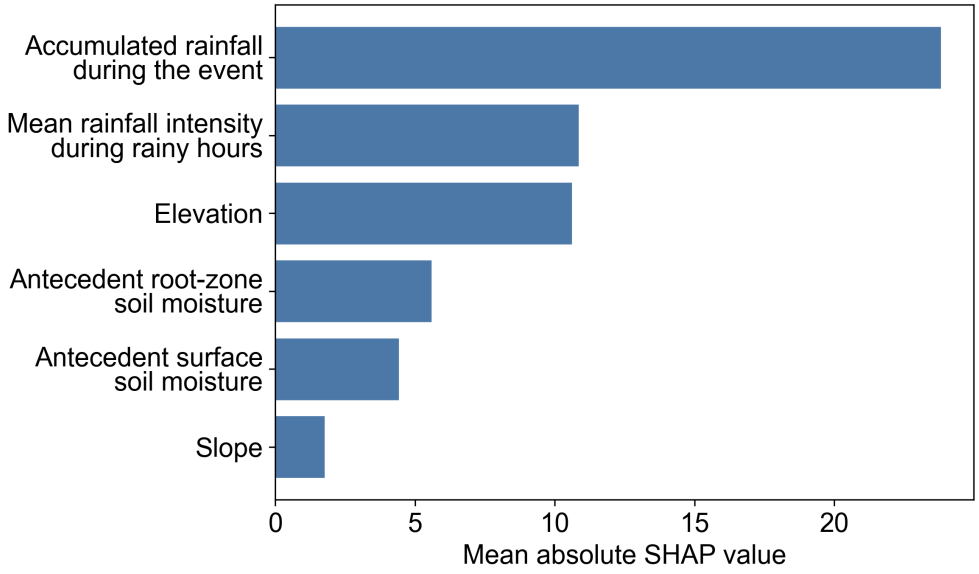

Figure 15. SHAP-based model importance of the selected explanatory variables in the drainage-duration model. The x-axis shows the mean absolute SHAP value for each variable, representing its average contribution to model predictions across all events, regardless of direction. Larger values indicate greater model-based predictive importance, rather than causal importance, in the fitted random-forest model.

Likewise, higher antecedent root-zone soil moisture was generally associated with longer predicted drainage duration, particularly across the lower-to-intermediate moisture range. This pattern suggests that wetter antecedent subsurface storage may provide a larger volume of water to be released or redistributed during drainage, thereby lengthening water-level recession and prolonging the time required for fields to reach drained conditions; this interpretation is consistent with the treatment of root-zone soil moisture as a deeper/profile storage state inferred from near-surface moisture dynamics rather than as an instantaneous surface-wetting signal [66]. However, the dependence became nonlinear toward the wetter end of the observed range, indicating that root-zone wetness should not be interpreted as having a simple linear effect across all conditions. Together, accumulated rainfall and antecedent root-zone soil moisture showed the clearest internally consistent model-based associations with drainage duration, linking event-period water input and pre-event subsurface storage to drainage persistence.

The effects of elevation, rainfall intensity, and antecedent surface soil moisture were more nuanced and require careful interpretation. Elevation showed a relatively strong contribution in the model (Figure 15), and the SHAP dependence pattern (Figure 16) suggests that lower-elevation fields tended to be associated with longer predicted drainage duration. This relationship is physically plausible in lowland rice systems, where small elevation differences and micro-relief can influence ponding, water stagnation, and the ease with which water moves toward drainage pathways [67]. However, elevation should not be interpreted as a direct measure of drainage efficiency. Rather, elevation is more likely acting as a landscape-position proxy that integrates several unobserved controls, including local depressional setting, hydraulic connectivity to drainage pathways, backwater influence, drainage infrastructure, and the broader spatial organization of lowland rice fields [68]. In addition, because drainage and runoff responses in paddy-field landscapes depend on broader watershed characteristics, including topography, land use, and drainage systems, the SHAP contribution of elevation may partly reflect spatial context rather than a transferable topographic effect [69]. In this sense, the elevation effect is best interpreted as a model-based indicator of spatial context, rather than as a simple topographic control operating uniformly across fields.

 doi:10.20944/preprints202604.2223.v1

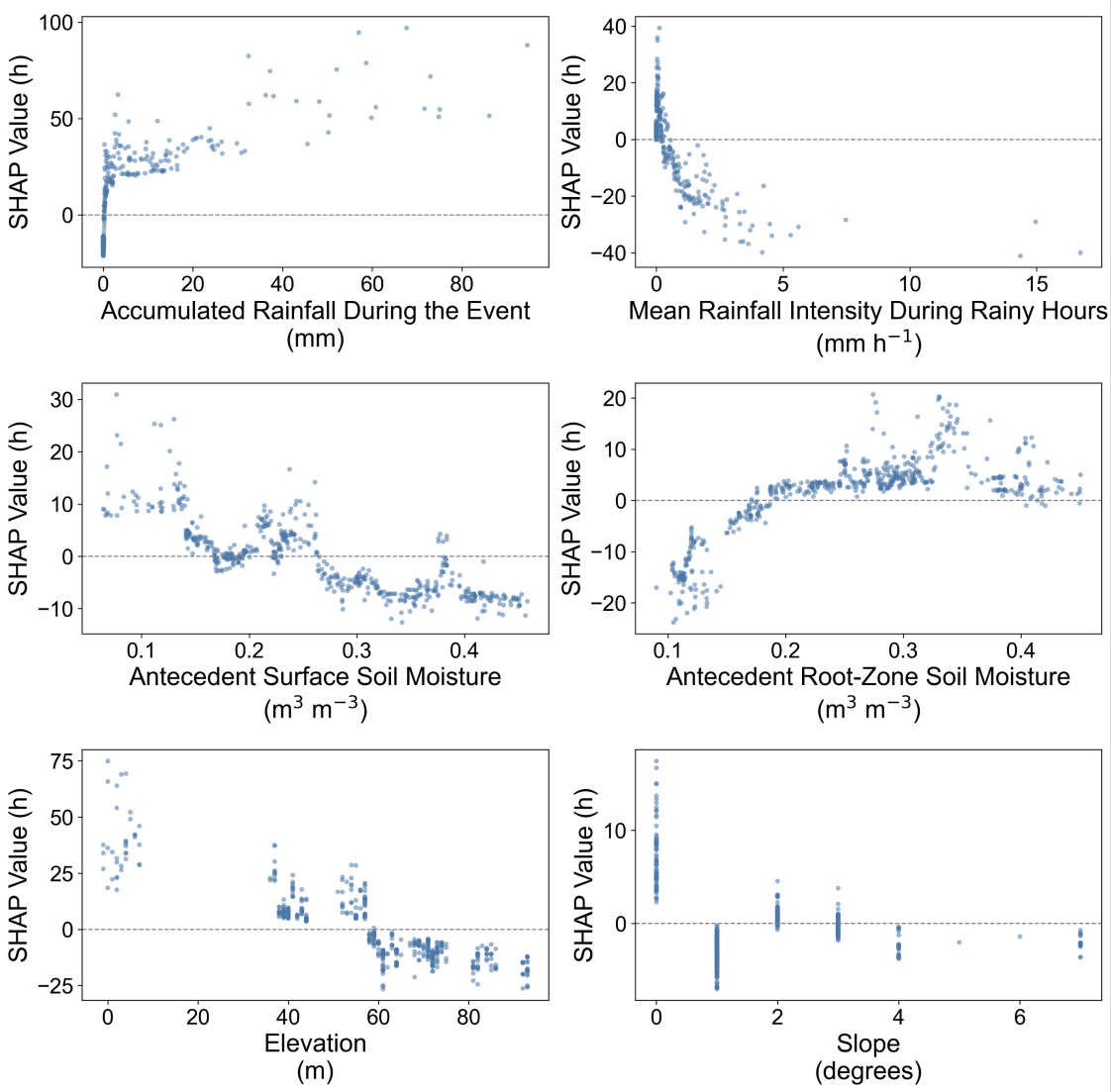

Figure 16. SHAP dependence plots for the selected explanatory variables in the drainage-duration model. The x-axis shows the observed value of each variable, and the y-axis shows its SHAP contribution to predicted drainage duration (h). Positive SHAP values indicate contributions toward longer predicted drainage duration, whereas negative values indicate contributions toward shorter predicted drainage duration.

Mean rainfall intensity during rainy hours also ranked relatively high, but its interpretation is less straightforward than that of accumulated rainfall. The SHAP dependence pattern suggested that higher mean rainfall intensity was often associated with lower SHAP contributions to predicted drainage duration, although the relationship was uneven and most observations were concentrated near low-intensity values. This apparent negative contribution should not be interpreted as evidence that intense rainfall directly shortened drainage duration. Rather, because accumulated rainfall was already included in the model, mean rainfall intensity likely represented the temporal concentration of rainfall input rather than water input magnitude alone. For a given amount of rainfall, higher active intensity may correspond to shorter, more pulse-like rainfall events, which can produce short-term water-level disturbances without necessarily sustaining prolonged drainage. By contrast, lower-intensity rainfall distributed over longer periods may be more effective in maintaining wet conditions and delaying recession. The dense cluster near zero also reflects events with little or no rainfall during the drainage period; for events with no rainy hours, active rainfall intensity was assigned a value of zero as a practical encoding of no event-period rainfall. In addition, the drainage-event definition constrained abrupt water-level jumps and short-term fluctuations, so events strongly disturbed by intense rainfall may have been split or excluded rather than retained as single continuous drainage

 doi:10.20944/preprints202604.2223.v1

episodes. Therefore, the importance of rainfall intensity should be interpreted as a model-based signal of rainfall temporal structure and event-selection sensitivity, rather than as a simple process-level effect.

A similarly cautious interpretation is needed for antecedent surface soil moisture. Although this variable contributed to the model, its dependence pattern was weaker and less physically intuitive than that of root-zone soil moisture. A likely reason is that surface soil moisture derived from coarse-resolution remote sensing products represents a short-term near-surface wetness signal that is highly sensitive to recent rainfall timing, surface evaporation, ponding, vegetation cover, and other near-surface conditions [66,70]. Its apparent effect may also be influenced indirectly by the event-selection process, because wetter near-surface conditions are more likely to coincide with rainfall-disturbed hydrographs. By contrast, root-zone soil moisture remained more stable and physically interpretable, suggesting that antecedent subsurface storage is a more robust indicator of drainage persistence than near-surface wetness alone. Therefore, the apparent surface-moisture effect should be treated as a context-dependent association rather than as a robust process-level relationship.

Slope showed the weakest contribution among the six variables, suggesting that the 30-m DEM-derived terrain gradient, as represented in this analysis, was not a dominant explanatory factor for drainage duration in the monitored fields. This should not be taken to mean that topography is unimportant. Rather, in bunded rice systems, a slope value derived from a 30-m DEM is an aggregated descriptor of terrain steepness and may not resolve the field-scale hydraulic features that regulate ponding and drainage. Previous work on paddy-field land leveling shows that small micro-relief anomalies can impede water movement and that field leveling, levee layout, and water-pass management can improve timely and homogeneous drainage [67]. Similarly, water-balance studies in flat, low-lying paddy areas emphasize that discharge dynamics are shaped by farm drains, drainage canals, lateral flow, backwater effects, pumping, and other water-control infrastructure [68,69]. Thus, microtopography, bund configuration, ditch connectivity, outlet condition, and active water-control practices may be more relevant to drainage behavior than the broader terrain gradient captured by the DEM-derived slope variable.

Several qualifications are important when interpreting these SHAP results. Because SHAP values describe contributions within the fitted model, the resulting importance ranking should be interpreted as model-based predictive importance rather than causal importance. This distinction is important because several predictors may be correlated, including accumulated rainfall and rainfall intensity, surface and root-zone soil moisture, and terrain variables that may also covary with region or field setting. Therefore, the SHAP results are best interpreted as identifying variables that carry predictive information within the fitted dataset, rather than as isolating independent causal effects.

The residual unexplained variation in drainage duration is also informative. Rainfall, antecedent wetness, and terrain together explained approximately half of the variation in the fitted model, suggesting that the remaining variation was influenced by additional factors not represented in the current analysis. In rice systems, these likely include irrigation scheduling, deliberate drainage management, bund manipulation, outlet control, crop growth stage, and local hydraulic connectivity [64,65,67]. Such controls are consistent with the observed seasonal and field-level heterogeneity discussed above, yet they were not available in a sufficiently consistent and accurate form for direct inclusion in the model. Since some fields contributed multiple events, the effective independence among observations may also be lower than the total number of detected events. Future analyses using field-level grouping, hierarchical models, or grouped validation would help separate event-scale variability from persistent field-level controls. The explanatory model should therefore be interpreted as identifying environmentally meaningful correlates of drainage duration, rather than as a complete accounting of all relevant controls.

Overall, the explanatory analysis indicates that drainage duration in the monitored rice fields cannot be understood solely as a function of antecedent wetness or rainfall amount in isolation. Instead, it appears to emerge from the combined influence of event-scale rainfall input, antecedent subsurface

 doi:10.20944/preprints202604.2223.v1

storage, and broader field setting, with additional modulation by unobserved management and penological factors. Because the SHAP dependence plots were not stratified by region or season, some apparent relationships may also reflect spatial or seasonal clustering among events. In this respect, the model is most valuable not as a predictive endpoint, but as a framework for identifying which remotely sensed environmental variables carry interpretable information on drainage persistence and which relationships remain conditional, indirect, or context dependent.

4.3. Field-Scale Hydrological Condition Determination with PALSAR-2

In Section 3.2.1, anomalously high backscatter observations acquired on 10 September 2024 were excluded from the analysis due to their suspected artefactual origin. Nevertheless, should these extreme values are confirmed to be valid, they may serve as reliable indicators of fields in semi-inundation conditions and motivate further investigation. Overall, the results presented in Figure 11 suggest that, while dual-polarization backscatter features capture general inundation-related trends, they are insufficient on their own for robust classification or determination or for determining the vertical distribution of field-scale water levels.

At first glance, defining a semi-inundation class spanning water levels from +40 to -110 mm may appear counterintuitive. However, this approach reflects the actual field conditions, where micro-topographic variability causes spatial heterogeneity in surface condition within the field. This heterogeneity results in mixed backscatter signals arising from surface water patches within the field (Figure 12). Consequently, the observed backscatter does not necessarily correspond to point-based in situ water level measurements. Therefore, adopting an inundation classification scheme that explicitly incorporates a transitional semi-inundated class, rather than relying solely on a fixed surface water threshold (0 mm), is more physically appropriate for operationally use of L-band SAR backscatter for detecting inundation conditions in paddy fields. However, this definition of semi-inundated condition differs from that of [21], which shows the SAR sensitivity for water in the shallow soil later up to 5 cm depth.

The results presented in Figure 11, Figure 13 and Figure 14 collectively highlight the strong influence of crop growth stage and field-scale variability on SAR backscatter. These effects arise from the interaction between canopy structure and underlying water condition. During the Early stage, the sparse and short rice canopy allows SAR signal to interact directly with the surface, and soil-water interactions dominate backscatter response. In full-inundated fields, specular reflection leads to lower co- and cross-polarized backscatter, whereas surface scattering dominates in non-inundated fields producing higher co-polarized backscatter. As the season progresses, the canopy development enhances volume scattering, increasing cross-polarized backscatter, as illustrated in Figure 14b. During the Late growth stage, in full-inundated fields the interaction between water-surface and rice stems promotes double-bounce scattering which is expected to eventually increase the co-polarized backscatter. However, this pattern is not clearly visible in Figure 14a, likely due to limited number of samples. Additionally, this could be attributed to the findings of [71], which indicate that rice plants exceeding approximately 70 cm in height can significantly attenuate backscatter contributions from the surface, thereby reducing inundation detection accuracy.

The ability to distinguish full-inundated from non-inundated paddies using SAR backscatter has direct operational relevance for monitoring drainage events associated with water-saving irrigation practices such as Alternate Wetting and Drying (AWD). AWD involves periodic drying and re-flooding of paddy fields also to reduce methane emissions, and timely confirmation of drainage events is critical for assessing AWD adoption and compliance at field scale. The results of this study suggest that HH and HV SAR polarizations holds potential for detecting such drainage transitions, particularly during the Mid growth stage Figure 14.

A key limitation of this study arises from the use of a one-sample t-test at the Late growth stage (Figure 14), reflecting the availability of only a single full-inundated sample. This is because the fields are intentionally kept non-inundated during the Late growth stage as a farming practice. This limitation constrains the statistical representativeness of the reference group. Increasing the

 doi:10.20944/preprints202604.2223.v1

number of full-inundated samples would improve the reliability of the analysis. Furthermore, the limitations of interpreting inundation status using dual-polarization SAR data alone are consistent with studies [21,26]. Incorporating full-polarization SAR data and adopting scattering component decomposition methods would likely enhance classification accuracy and support more reliable operational applications [21,26,72].

5. Conclusions

Using a large set of in situ sensor-based water-level records from monitored rice fields, this study quantified field-scale drainage dynamics relevant to AWD and evaluated the sensitivity of open-access dual-polarization PALSAR-2 observations to hydrological transitions in paddy fields.

Our in situ sensor observations show that, under farmer-managed field conditions, drainage from near-surface water levels to approximately 15 cm below the soil surface generally occurred within hours to a few days, rather than over a fixed multi-day interval. Across 564 detected drainage events, the median duration was 19.0 h, and only five events (0.9%) exceeded 240 h, indicating that events longer than 240 h accounted for only a small fraction of the observed drainage events. However, drainage behavior was highly heterogeneous across regions and seasons. Pangasinan was dominated by short-duration events, whereas Chiba and Cagayan showed relatively longer drainage-duration profiles. In Pangasinan, dry-season events were longer and recurred more frequently than wet-season events, suggesting that seasonal water management and field-specific conditions influenced both drainage duration and drainage frequency. These findings indicate that AWD-related drainage dynamics are strongly site- and season-dependent, highlighting the need for location-specific interpretation rather than a single universal drainage-duration assumption.

The field-scale applicability of open-access PALSAR-2 L2.2 ScanSAR dual-polarization backscatter was evaluated for detecting inundation conditions across three classes; full-, semi-, and non-inundated defined using coincident in situ water-level observations. Backscatter signals broadly followed theoretically expected trends with crop development, yet the three inundation classes exhibited substantial overlap across all growth stages in HH-HV feature space. A semi-inundation zone was introduced to account for micro-topographic heterogeneity within fields and moist-soil appearance at shallow water-level beneath the surface, where mixed scattering mechanisms complicate direct correspondence between point-based water-level measurements and field-scale backscatter. Statistically significant differences between full- and non-inundated conditions were observed for HV backscatter during the Mid growth stage and for the HH/HV ratio across all stages combined, but class separation remained insufficient for reliable standalone discrimination. These findings indicate that dual-polarization L-band SAR alone cannot robustly resolve the hydrological transitions relevant to AWD monitoring. Incorporation of full-polarization data with scattering decomposition methods is recommended to improve classification reliability.

Supplementary Materials: The following supporting information can be downloaded at the website of this paper posted on Preprints.org.

Author Contributions: Conceptualization, X.J., M.M.D. and A.D.; methodology, X.J. and M.M.D.; software, X.J. and M.M.D.; validation, X.J. and M.M.D.; formal analysis, X.J. and M.M.D.; investigation, X.J. and M.M.D.; resources, A.D.; data curation, X.J. and M.M.D.; writing—original draft preparation, X.J. and M.M.D.; writing—review and editing, X.J., M.M.D. and A.D.; visualization, X.J. and M.M.D.; supervision, A.D., S.K. and A.C.G.V.; project administration, A.D.; funding acquisition, S.K. and A.C.G.V. All authors have read and agreed to the published version of the manuscript.

Funding: This research was funded by JSPS KAKENHI Grant Numbers JP21K14249, JP25K00040 and by JST SPRING, Japan Grant Number JPMJSP2180.

Data Availability Statement: Raw satellite images from PALSAR-2 ScanSAR Level 2.2 are accessible in the Google Earth Engine platform. Water level measurements can be requested from Creattura Co., Ltd.

 doi:10.20944/preprints202604.2223.v1

Acknowledgments: The authors would like to express their sincere gratitude to the anonymous reviewers for their valuable comments and suggestions. The authors also acknowledge Rayson Florendo for his dedicated efforts in maintaining the in situ water-level sensors, and Creattura Co., Ltd. for their trust and support in providing the water-level measurements used in this study. During the preparation of this manuscript, the authors used a language assistance tool to improve writing quality. The authors have carefully reviewed and edited the output and take full responsibility for the content of this publication. In addition, Anthropic Claude Sonnet 4.6 was used to assist in preparing Figure S5, where data were extracted from the original figure published in [23]. The authors have verified the results and take full responsibility for the accuracy and integrity of the reproduced content.

Conflicts of Interest: The authors declare no conflict of interest regarding the contents or results presented in the manuscript. Although Alexis Declaro is affiliated with Creattura Co., Ltd., the company had no role in the design, execution, interpretation or reporting of this study.

References

1. Xuan, T.D.; Minh, T.T.N.; Rayee, R.; Dong, N.D.; Chien, N.X. Advances in mitigating methane emissions from rice cultivation: past, present, and future strategies. *Environmental Science and Pollution Research* **2025**, *32*, 20232–20247.
2. Saunois, M.; Martinez, A.; Poulter, B.; Zhang, Z.; Raymond, P.A.; Regnier, P.; Canadell, J.G.; Jackson, R.B.; Patra, P.K.; Bousquet, P.; et al. Global methane budget 2000–2020. *Earth System Science Data* **2025**, *17*, 1873–1958.
3. Intergovernmental Panel on Climate Change. Chapter 5: Cropland. In *2019 Refinement to the 2006 IPCC Guidelines for National Greenhouse Gas Inventories, Volume 4: Agriculture, Forestry and Other Land Use*; IPCC/IGES: Hayama, Japan, 2019.
4. Bouman, B.A.M.; Lampayan, R.M.; Tuong, T.P. *Water Management in Irrigated Rice: Coping with Water Scarcity*; International Rice Research Institute: Los Baños, Philippines, 2007.
5. Lampayan, R.M.; Rejesus, R.M.; Singleton, G.R.; Bouman, B.A. Adoption and economics of alternate wetting and drying water management for irrigated lowland rice. *Field Crops Research* **2015**, *170*, 95–108.
6. Howell, K.R.; Shrestha, P.; Dodd, I.C. Alternate wetting and drying irrigation maintained rice yields despite half the irrigation volume, but is currently unlikely to be adopted by smallholder lowland rice farmers in Nepal. *Food and energy security* **2015**, *4*, 144–157.
7. Carrijo, D.R.; Lundy, M.E.; Linquist, B.A. Rice yields and water use under alternate wetting and drying irrigation: A meta-analysis. *Field Crops Research* **2017**, *203*, 173–180.
8. Setyanto, P.; Pramono, A.; Adriany, T.A.; Susilawati, H.L.; Tokida, T.; Padre, A.T.; Minamikawa, K. Alternate wetting and drying reduces methane emission from a rice paddy in Central Java, Indonesia without yield loss. *Soil Science and Plant Nutrition* **2018**, *64*, 23–30. https://doi.org/10.1080/00380768.2017.1409600.
9. Tran, D.H.; Hoang, T.N.; Tokida, T.; Tirol-Padre, A.; Minamikawa, K. Impacts of alternate wetting and drying on greenhouse gas emission from paddy field in Central Vietnam. *Soil Science and Plant Nutrition* **2018**, *64*, 14–22. https://doi.org/10.1080/00380768.2017.1409601.
10. Sibayan, E.B.; Samoy-Pascual, K.; Grospe, F.S.; Casil, M.E.D.; Tokida, T.; Padre, A.T.; Minamikawa, K. Effects of alternate wetting and drying technique on greenhouse gas emissions from irrigated rice paddy in Central Luzon, Philippines. *Soil Science and Plant Nutrition* **2018**, *64*, 39–46. https://doi.org/10.1080/00380768.2017.1401906.
11. Jiang, Y.; Carrijo, D.; Huang, S.; Chen, J.; Balaine, N.; Zhang, W.; van Groenigen, K.J.; Linquist, B.A. Water management to mitigate the global warming potential of rice systems: A global meta-analysis. *Field Crops Research* **2019**, *234*, 47–54. https://doi.org/10.1016/j.fcr.2019.02.010.
12. Carrijo, D.R.; Lundy, M.E.; Linquist, B.A. Rice yields and water use under alternate wetting and drying irrigation: A meta-analysis. *Field Crops Research* **2017**, *203*, 173–180. https://doi.org/10.1016/j.fcr.2016.12.002.
13. Lampayan, R.; Samoy-Pascual, K.; Sibayan, E.; Ella, V.; Jayag, O.; Cabangon, R.; Bouman, B. Effects of alternate wetting and drying (AWD) threshold level and plant seedling age on crop performance, water input, and water productivity of transplanted rice in Central Luzon, Philippines. *Paddy and Water Environment* **2015**, *13*, 215–227.
14. Rahman, M.R.; Bulbul, S.H. Effect of Alternate Wetting and Drying (AWD) Irrigation for Boro Rice Cultivation in Bangladesh. *Agriculture, Forestry and Fisheries* **2014**, *3*, 86–92. https://doi.org/10.11648/j.aff.20140302.16.

 doi:10.20944/preprints202604.2223.v1

15. Rejesus, R.M.; Palis, F.G.; Rodriguez, D.G.P.; Lampayan, R.M.; Bouman, B.A. Impact of the alternate wetting and drying (AWD) water-saving irrigation technique: Evidence from rice producers in the Philippines. *Food Policy* **2011**, *36*, 280–288.
16. Chapagain, T.; Riseman, A.; Yamaji, E. Achieving more with less water: Alternate wet and dry irrigation (AWDI) as an alternative to the conventional water management practices in rice farming. *Journal of Agricultural Science* **2011**, *3*, 3.
17. Kuo, S.F. Evaluation of irrigation water requirements and crop yields with different irrigation schedules for paddy fields in ChiaNan irrigated area, Taiwan. *Paddy and water environment* **2014**, *12*, 71–78.
18. Pascual, V.J.; Wang, Y.M. Impact of water management on rice varieties, yield, and water productivity under the system of rice intensification in Southern Taiwan. *Water* **2016**, *9*, 3.
19. Xu, B.; Shao, D.; Tan, X.; Yang, X.; Gu, W.; Li, H. Evaluation of soil water percolation under different irrigation practices, antecedent moisture and groundwater depths in paddy fields. *Agricultural Water Management* **2017**, *192*, 149–158. https://doi.org/10.1016/j.agwat.2017.06.002.
20. Arenas-Calle, L.; Sherpa, S.R.; Rossiter, D.G.; Nayak, H.; Urfels, A.; Kritee, K.; Poonia, S.; Singh, D.K.; Choudhary, A.; Dubey, R.; et al. Hydrologic variability governs GHG emissions in rice-based cropping systems of Eastern India. *Agricultural Water Management* **2024**, *301*, 108931. https://doi.org/10.1016/j.agwat.2024.108931.
21. Arai, H.; Le Toan, T.; Takeuchi, W.; Oyoshi, K.; Fumoto, T.; Inubushi, K. Evaluating irrigation status in the Mekong Delta through polarimetric L-band SAR data assimilation. *Remote Sensing of Environment* **2022**, *279*, 113139. https://doi.org/https://doi.org/10.1016/j.rse.2022.113139.
22. Hoshikawa, K.; Phontusang, P.; Katawatin, R. Synthetic aperture radar polarised backscattering behaviour in partially inundated agricultural fields. *European Journal of Remote Sensing* **2023**, *56*, 2269305, [https://doi.org/10.1080/22797254.2023.2269305]. https://doi.org/10.1080/22797254.2023.2269305.
23. Inoue, Y.; Kurosu, T.; Maeno, H.; Uratsuka, S.; Kozu, T.; Dabrowska-Zielinska, K.; Qi, J. Season-long daily measurements of multifrequency (Ka, Ku, X, C, and L) and full-polarization backscatter signatures over paddy rice field and their relationship with biological variables. *Remote Sensing of Environment* **2002**, *81*, 194–204. https://doi.org/https://doi.org/10.1016/S0034-4257(01)00343-1.
24. Torbick, N.; Chowdhury, D.; Salas, W.; Qi, J. Monitoring Rice Agriculture across Myanmar Using Time Series Sentinel-1 Assisted by Landsat-8 and PALSAR-2. *Remote Sensing* **2017**, *9*. https://doi.org/10.3390/rs9020119.
25. Wang, C.; Wu, J.; Zhang, Y.; Pan, G.; Qi, J.; Salas, W.A. Characterizing L-Band Scattering of Paddy Rice in Southeast China With Radiative Transfer Model and Multitemporal ALOS/PALSAR Imagery. *IEEE Transactions on Geoscience and Remote Sensing* **2009**, *47*, 988–998. https://doi.org/10.1109/TGRS.2008.2008309.
26. Arai, H.; Takeuchi, W.; Oyoshi, K.; Nguyen, L.D.; Inubushi, K. Estimation of Methane Emissions from Rice Paddies in the Mekong Delta Based on Land Surface Dynamics Characterization with Remote Sensing. *Remote Sensing* **2018**, *10*. https://doi.org/10.3390/rs10091438.
27. Mirandilla, J.R.F.; Yamashita, M.; Yoshimura, M. Phenological Monitoring and Discrimination of Rice Ecosystems Using Multi-Temporal and Multi-Sensor Polarimetric SAR. *Remote Sensing* **2025**, *17*. https://doi.org/10.3390/rs17244007.
28. Ling, F.; Li, Z.; Chen, E.; Tian, X.; Bai, L.; Wang, F. Rice areas mapping using ALOS PALSAR FBD data considering the Bragg scattering in L-band SAR images of rice fields. In Proceedings of the 2010 IEEE International Geoscience and Remote Sensing Symposium, 2010, pp. 1461–1464. https://doi.org/10.1109/IGARSS.2010.5653328.
29. Zhang, Y.; Wang, C.; Zhang, Q. Identifying paddy fields with dual-polarization ALOS/PALSAR data. *Canadian Journal of Remote Sensing* **2011**, *37*, 103–111, [https://doi.org/10.5589/m11-016]. https://doi.org/10.5589/m11-016.
30. Sander, B.O.; Wassmann, R.; Palao, L.K.; Nelson, A. Climate-based suitability assessment for alternate wetting and drying water management in the Philippines: a novel approach for mapping methane mitigation potential in rice production. *Carbon management* **2017**, *8*, 331–342.
31. Bartelet, H.A.; Prodigalidad, A.J.D.; Dy, J.S.; Manzano, J.G.N. Understanding rice production stagnation in the Philippines: Regional evidence and development implications. *PLoS One* **2025**, *20*, e0335344.
32. Gutierrez, M.; Paguirigan, N.; Raviz, J.; Mabalay, M.; Alosnos, E.; Villano, L.; Asilo, S.; Arocena Jr, A.; Maloom, J.; Laborte, A. The rice planting window in the Philippines: an analysis using multi-temporal SAR imagery. *The International Archives of the Photogrammetry, Remote Sensing and Spatial Information Sciences* **2019**, *42*, 241–248.

 doi:10.20944/preprints202604.2223.v1

33. Aoki, Y.; Mochizuki, A.; Nakamura, M.; Kuwata, C. Development and Field Validation of a Smartphone-Based Web Application for Diagnosing Optimal Timing of Mid-Season Drainage in Rice Cultivation via Canopy Image-Derived Tiller Estimation. *Sensors* **2026**, *26*, 1000.
34. Chapagain, T.; Yamaji, E. The effects of irrigation method, age of seedling and spacing on crop performance, productivity and water-wise rice production in Japan. *Paddy and water environment* **2010**, *8*, 81–90.
35. Mabalay, M.R.; Raviz, J.; Alosnos, E.; Barbieri, M.; Quicho, E.; Bibar, J.E.A.; Barroga, M.; Coñado, M.; Mabalot, P.; Mirandilla, J.R.; et al. The Philippine rice information system (PRiSM): an operational monitoring and information system on rice. In *Remote sensing of agriculture and land cover/land use changes in South and Southeast Asian countries*; Springer, 2022; pp. 133–150.
36. Dunn, O.J. Multiple Comparisons Using Rank Sums. *Technometrics* **1964**, *6*, 241–252. https://doi.org/10.1080/00401706.1964.10490181.
37. Holm, S. A Simple Sequentially Rejective Multiple Test Procedure. *Scand. J. Stat.* **1979**, *6*, 65–70.
38. Mann, H.B.; Whitney, D.R. On a Test of Whether One of Two Random Variables Is Stochastically Larger than the Other. *Ann. Math. Stat.* **1947**, *18*, 50–60. https://doi.org/10.1214/aoms/1177730491.
39. Benjamini, Y.; Hochberg, Y. Controlling the False Discovery Rate: A Practical and Powerful Approach to Multiple Testing. *J. R. Stat. Soc. Ser. B Methodol.* **1995**, *57*, 289–300. https://doi.org/10.1111/j.2517-6161.1995.tb02031.x.
40. Gorelick, N.; Hancher, M.; Dixon, M.; Ilyushchenko, S.; Thau, D.; Moore, R. Google Earth Engine: Planetary-Scale Geospatial Analysis for Everyone. *Remote Sens. Environ.* **2017**, *202*, 18–27. https://doi.org/10.1016/j.rse.2017.06.031.
41. Kubota, T.; Aonashi, K.; Ushio, T.; Shige, S.; Takayabu, Y.N.; Kachi, M.; Arai, Y.; Tashima, T.; Masaki, T.; Kawamoto, N.; et al. Global Satellite Mapping of Precipitation (GSMaP) Products in the GPM Era. In *Satellite Precipitation Measurement*; Springer: Cham, Switzerland, 2020; Vol. 67, *Advances in Global Change Research*, pp. 355–373. https://doi.org/10.1007/978-3-030-24568-9_20.
42. Kubota, T.; Shige, S.; Hashizume, H.; Aonashi, K.; Takahashi, N.; Seto, S.; Hirose, M.; Takayabu, Y.N.; Nakagawa, K.; Iwanami, K.; et al. Global Precipitation Map Using Satellite-Borne Microwave Radiometers by the GSMaP Project: Production and Validation. *IEEE Trans. Geosci. Remote Sens.* **2007**, *45*, 2259–2275. https://doi.org/10.1109/TGRS.2007.895337.
43. Aonashi, K.; Awaka, J.; Hirose, M.; Kozu, T.; Kubota, T.; Liu, G.; Shige, S.; Kida, S.; Seto, S.; Takahashi, N.; et al. GSMaP Passive Microwave Precipitation Retrieval Algorithm: Algorithm Description and Validation. *J. Meteorol. Soc. Jpn. Ser. II* **2009**, *87A*, 119–136. https://doi.org/10.2151/jmsj.87A.119.
44. Ushio, T.; Sasashige, K.; Kubota, T.; Shige, S.; Okamoto, K.; Aonashi, K.; Inoue, T.; Takahashi, N.; Iguchi, T.; Kachi, M.; et al. A Kalman Filter Approach to the Global Satellite Mapping of Precipitation (GSMaP) from Combined Passive Microwave and Infrared Radiometric Data. *J. Meteorol. Soc. Jpn. Ser. II* **2009**, *87A*, 137–151. https://doi.org/10.2151/jmsj.87A.137.
45. Reichle, R.H.; Liu, Q.; Koster, R.D.; Crow, W.T.; De Lannoy, G.J.M.; Kimball, J.S.; Ardizzone, J.V.; Bosch, D.; Colliander, A.; Cosh, M.; et al. Version 4 of the SMAP Level-4 Soil Moisture Algorithm and Data Product. *J. Adv. Model. Earth Syst.* **2019**, *11*, 3106–3130. https://doi.org/10.1029/2019MS001729.
46. Reichle, R.H.; De Lannoy, G.J.M.; Liu, Q.; Ardizzone, J.V.; Colliander, A.; Conaty, A.; Crow, W.; Jackson, T.J.; Jones, L.A.; Kimball, J.S.; et al. Assessment of the SMAP Level-4 Surface and Root-Zone Soil Moisture Product Using In Situ Measurements. *J. Hydrometeorol.* **2017**, *18*, 2621–2645. https://doi.org/10.1175/JHM-D-17-0063.1.
47. Farr, T.G.; Rosen, P.A.; Caro, E.; Crippen, R.; Duren, R.; Hensley, S.; Kobrick, M.; Paller, M.; Rodriguez, E.; Roth, L.; et al. The Shuttle Radar Topography Mission. *Rev. Geophys.* **2007**, *45*, RG2004. https://doi.org/10.1029/2005RG000183.
48. Friedman, J.H. Greedy Function Approximation: A Gradient Boosting Machine. *Ann. Stat.* **2001**, *29*, 1189–1232. https://doi.org/10.1214/aos/1013203451.
49. Ke, G.; Meng, Q.; Finley, T.; Wang, T.; Chen, W.; Ma, W.; Ye, Q.; Liu, T.Y. LightGBM: A Highly Efficient Gradient Boosting Decision Tree. In Proceedings of the Advances in Neural Information Processing Systems 30. Curran Associates, Inc., 2017, pp. 3146–3154.
50. Willmott, C.J.; Matsuura, K. Advantages of the Mean Absolute Error (MAE) over the Root Mean Square Error (RMSE) in Assessing Average Model Performance. *Clim. Res.* **2005**, *30*, 79–82. https://doi.org/10.3354/cr030079.

 doi:10.20944/preprints202604.2223.v1

51. Chai, T.; Draxler, R.R. Root Mean Square Error (RMSE) or Mean Absolute Error (MAE)? Arguments against Avoiding RMSE in the Literature. *Geosci. Model Dev.* **2014**, *7*, 1247–1250. https://doi.org/10.5194/gmd-7-1247-2014.
52. Lundberg, S.M.; Lee, S.I. A Unified Approach to Interpreting Model Predictions. In Proceedings of the Advances in Neural Information Processing Systems 30. Curran Associates, Inc., 2017, pp. 4765–4774.
53. Lundberg, S.M.; Erion, G.; Chen, H.; DeGrave, A.; Prutkin, J.M.; Nair, B.; Katz, R.; Himmelfarb, J.; Bansal, N.; Lee, S.I. From Local Explanations to Global Understanding with Explainable AI for Trees. *Nat. Mach. Intell.* **2020**, *2*, 56–67. https://doi.org/10.1038/s42256-019-0138-9.
54. (EORC), J.E.O.R.C. *PALSAR-2 Level 2.2 - Normalised Radar Backscatter of the Analysis Ready Data for Land (CARD4L) Product Format Description*. Japan Aerospace Exploration Agency (JAXA), 2022. Version 1.0 (July 15, 2022).
55. Winkler, A.S.; Silva, J.T.d.; Parfitt, J.; Teixeira-Gandra, C.F.; Conceço, G.; Timm, L.C. Surface drainage in leveled land: Implication of slope. *Revista Brasileira de Engenharia Agrícola e Ambiental* **2018**, *22*, 77–82.
56. Liu, L.; Ouyang, W.; Liu, H.; Zhu, J.; Fan, X.; Zhang, F.; Ma, Y.; Chen, J.; Hao, F.; Lian, Z. Drainage optimization of paddy field watershed for diffuse phosphorus pollution control and sustainable agricultural development. *Agriculture, Ecosystems & Environment* **2021**, *308*, 107238.
57. Khanh, P.T.; Pramanik, S.; Ngoc, T.T.H. Soil permeability of sandy loam and clay loam soil in the paddy fields in An Giang Province in Vietnam. *Environmental Challenges* **2024**, *15*, 100907.
58. Huang, C.L.; Huang, H.L.; Hsu, N.S.; Chen, C.W. Optimization of bund wall height and trigger depth for re-irrigation in paddy field by deepwater ponding irrigation treatment. *Irrigation and Drainage* **2020**, *69*, 584–602.
59. Phoeurn, C.A.; Orn, C.; Tho, T.; Oeurng, C.; Degré, A.; Ket, P. Assessing the feasibility of alternate wetting and drying (AWD) technique for improving water use efficiency in dry-season rice production. *Paddy and Water Environment* **2025**, *23*, 229–242.
60. Rejesus, R.M.; Palis, F.G.; Rodriguez, D.G.P.; Lampayan, R.M.; Bouman, B.A. Impact of the alternate wetting and drying (AWD) water-saving irrigation technique: Evidence from rice producers in the Philippines. *Food Policy* **2011**, *36*, 280–288.
61. Lampayan, R.M.; Rejesus, R.M.; Singleton, G.R.; Bouman, B.A. Adoption and economics of alternate wetting and drying water management for irrigated lowland rice. *Field Crops Research* **2015**, *170*, 95–108.
62. Bhuiyan, S.; Undan, R. Drainage in rice culture in the Asian humid tropics. In Proceedings of the Paper presented, 1986.
63. Yamaguchi, T.; Minamikawa, K.; Yokoyama, S. Alternate wetting and drying (AWD) irrigation technology uptake in rice paddies of the Mekong Delta, Vietnam: Relationship between local conditions and the practiced technology. *Asian and African Area Studies* **2016**, *15*, 234–256.
64. Jung, J.W.; Yoon, K.S.; Choi, D.H.; Lim, S.S.; Choi, W.J.; Choi, S.M.; Lim, B.J. Water management practices and SCS curve numbers of paddy fields equipped with surface drainage pipes. *Agricultural Water Management* **2012**, *110*, 78–83.
65. Li, S.; Zhuang, Y.; Liu, H.; Wang, Z.; Zhang, F.; Lv, M.; Zhai, L.; Fan, X.; Niu, S.; Chen, J.; et al. Enhancing rice production sustainability and resilience via reactivating small water bodies for irrigation and drainage. *Nature Communications* **2023**, *14*, 3794.
66. Albergel, C.; Rüdiger, C.; Pellarin, T.; Calvet, J.C.; Fritz, N.; Froissard, F.; Suquia, D.; Petitpa, A.; Piguet, B.; Martin, E. From near-surface to root-zone soil moisture using an exponential filter: an assessment of the method based on in-situ observations and model simulations. *Hydrology and Earth System Sciences* **2008**, *12*, 1323–1337.
67. Quirós-Vargas, J.; Romanelli, T.L.; Rascher, U.; Agüero, J. Sustainability performance through technology adoption: a case study of land leveling in a paddy field. *Agronomy* **2020**, *10*, 1681.
68. Okura, F.; Kamei, A.; Kato, T. Water balance analysis of hydrological processes in cyclic irrigation: A case study of the Imbanuma irrigation area in Chiba, Japan. *Journal of Hydrology: Regional Studies* **2025**, *57*, 102111.
69. Yoshikawa, N.; Nagao, N.; Misawa, S. Evaluation of the flood mitigation effect of a Paddy Field Dam project. *Agricultural Water Management* **2010**, *97*, 259–270.
70. Babaeian, E.; Sadeghi, M.; Jones, S.B.; Montzka, C.; Vereecken, H.; Tuller, M. Ground, proximal, and satellite remote sensing of soil moisture. *Reviews of Geophysics* **2019**, *57*, 530–616.

 doi:10.20944/preprints202604.2223.v1

71. Segami, G.; Oyoshi, K.; Sobue, S.; Takeuchi, W. Characterizing L-Band Backscatter in Inundated and Non-Inundated Rice Paddies for Water Management Monitoring. *Remote Sensing* **2026**, *18*. https://doi.org/10.3390/rs18020370.
72. Huang, X.; Runkle, B.R.K.; Isbell, M.; Moreno-García, B.; McNairn, H.; Reba, M.L.; Torbick, N. Rice Inundation Assessment Using Polarimetric UAVSAR Data. *Earth and Space Science* **2021**, *8*, e2020EA001554. https://doi.org/https://doi.org/10.1029/2020EA001554.